Cell

Pseudouridine RNA avoids immune detection through impaired endolysosomal processing and TLR engagement

Graphical abstract

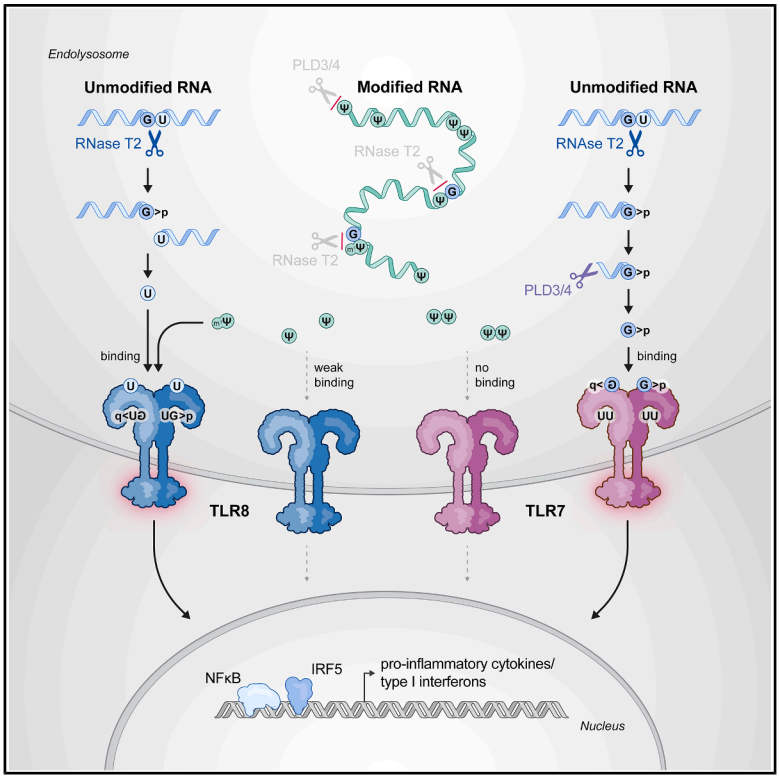

Highlights

- The non-immunogenicity of Ψ-RNA results from poor processing by lysosomal nucleases
- RNase T2 and PLDs fail to generate TLR7 and TLR8 ligands from Ψ-modified RNA
- Ψ and Ψ-RNA poorly engage distinct ligand-binding pockets of TLR8 and TLR7
- $m^1\Psi$ evades nuclease cleavage but could activate TLR8 if released from RNA

Authors

Marleen Bérouti, Mirko Wagner, Wilhelm Greulich, ..., Michael Sattler, Thomas Carell, Veit Hornung

Correspondence

thomas.carell@cup.uni-muenchen.de (T.C.), veit.hornung@lmu.de (V.H.)

In brief

Toll-like receptors (TLRs) 7 and 8 detect RNA degradation products to sense infection. However, modified nucleosides common in self-RNA—most notably pseudouridine—evade recognition. This study finds that poor nuclease processing and selective TLR avoidance drive this evasion, offering insight into the molecular basis of immune tolerance to pseudouridine-containing RNA.

Bérouti et al., 2025, Cell *188*, 1–16
September 4, 2025
https://doi.org/10.1016/j.cell.2025.05.032

CellPress

Please cite this article in press as: Bérouti et al., Pseudouridine RNA avoids immune detection through impaired endolysosomal processing and TLR engagement, Cell (2025), https://doi.org/10.1016/j.cell.2025.05.032

Cell

CellPress
OPEN ACCESS

Article

Pseudouridine RNA avoids immune detection through impaired endolysosomal processing and TLR engagement

Marleen Bérouti,[1,7] Mirko Wagner,[2,7] Wilhelm Greulich,[1] Ignazio Piseddu,[1,3,4] Jan Gärtig,[4] Larissa Hansbauer,[1] Christoph Müller-Hermes,[5,6] Matthias Heiss,[2] Alexander Pichler,[2] Annika J. Tölke,[2] Gregor Witte,[1] Karl-Peter Hopfner,[1] David Anz,[3,4] Michael Sattler,[5,6] Thomas Carell,[2,*] and Veit Hornung[1,8,*]

[1]Gene Center and Department of Biochemistry, Ludwig-Maximilians-Universität, Munich, Germany
[2]Department of Chemistry, Ludwig-Maximilians-Universität, Munich, Germany
[3]Department of Medicine II, LMU University Hospital, Ludwig-Maximilians-Universität, Munich, Germany
[4]Division of Clinical Pharmacology, LMU University Hospital, Ludwig-Maximilians-Universität, Munich, Germany
[5]Institute of Structural Biology, Helmholtz Munich, Neuherberg, Germany
[6]TUM School of Natural Sciences, Bavarian NMR Center and Department of Bioscience, Technical University of Munich, Garching, Germany
[7]These authors contributed equally
[8]Lead contact
*Correspondence: thomas.carell@cup.uni-muenchen.de (T.C.), veit.hornung@lmu.de (V.H.)
https://doi.org/10.1016/j.cell.2025.05.032

SUMMARY

Recognition of exogenous RNA by Toll-like receptors (TLRs) is central to pathogen defense. Using two distinct binding pockets, TLR7 and TLR8 recognize RNA degradation products generated by endolysosomal nucleases. RNA modifications present in endogenous RNA prevent TLR activation; notably, pseudouridine-containing RNA lacks immunostimulatory activity. Indeed, this property has been critical to the successful implementation of mRNA technology for medical purposes. However, the molecular mechanism for this immune evasion has remained elusive. Here, we report that RNase T2 and PLD exonucleases do not adequately process pseudouridine-containing RNA to generate TLR-agonistic ligands. As a second safety mechanism, TLR8 neglects pseudouridine as a ligand for its first binding pocket and TLR7 neglects pseudouridine-containing RNA as a ligand for its second pocket. Interestingly, the medically used N1-methylpseudouridine also evades RNase T2, PLD3, and PLD4 processing but is able to directly activate TLR8. Taken together, our findings provide a molecular basis for self-avoidance by RNA-sensing TLRs.

INTRODUCTION

Pattern recognition receptors (PRRs) are integral to the innate immune system's ability to recognize and respond to infectious agents. Among various receptor families, Toll-like receptors (TLRs) belong to the best characterized PRRs. TLRs are expressed as transmembrane receptors with their LRR (leucine rich repeat) ligand-binding domain either facing the extracellular space or the luminal compartment. A distinct evolutionary subgroup of TLRs, located in the endolysosomal compartment, is specialized in sensing nucleic acids, which constitutes a critical function in defense against viral and bacterial pathogens.[1] In the human system this group includes TLR7 and TLR8 that have evolved to recognize RNA degradation products[2] and TLR9 that senses single-stranded DNA with unmethylated cytosine and guanine (CG) motifs.[3] TLR7 and TLR8 are characterized by two distinct binding sites that function in a cooperative manner. The presence of a single-stranded RNA (ssRNA) fragment in binding pocket 2 allosterically regulates the affinity of the first binding pocket for its respective nucleoside or nucleotide ligand: TLR8 recognizes uridine (U) in combination with short purine (R)-terminated ssRNA fragments,[4] while TLR7 binds guanosine (G) or a 2′,3′-cyclophosphate-guanosine (2′,3′-cGMP or G>p) together with short pyrimidine-rich fragments.[5,6]

The production of the relevant RNA ligands for TLR7 and TLR8 is a regulated process in which the lysosomal endonuclease RNase T2 is non-redundantly involved. Human RNase T2 cleaves ssRNA, preferring R-U motifs (5′-$N_nR{\downarrow}UN_n$-3′), thus generating fragments with a 2′,3′-cyclophosphate-R at one end (5′-N_nR>p) and a 5′-hydroxyl-U at the other end (UN_n-3′).[7] The former fragment binds to the second pocket of TLR8, while the UN_n-3′ fragment undergoes exonucleolytic degradation, potentially via PLD3 or PLD4 exonucleases, thereby increasing the lysosomal U concentration required for the engagement of pocket 1. The reverse scenario is true for TLR7: here, the RNase T2 generated 2′,3′-cyclophosphate-guanosine terminated RNA fragments constitute substrate for the exonucleases PLD3 and PLD4 that degrade the RNA to release the terminal 2′,3′-cyclic

GMP to engage pocket 1. In addition, PLD3 and PLD4 activity also contributes to generate short RNA fragments that occupy the second binding pocket.[8]

Pseudouridine (Ψ), first identified in the early 1950s, is the most abundant naturally occurring modification within RNA, making up to 9% of the U pool of total RNA.[9] Chemically, Ψ is a U isomer characterized as a C-glycoside in which the β-D-ribose is attached to the C5 atom rather than the N1 atom of uracil. This small but significant structural change confers distinctive biophysical and biochemical properties on RNA molecules, notably enhanced base stacking and pairing capabilities. Ψ is ubiquitously present in various endogenous RNAs, including tRNA, rRNA, mRNA, and small nuclear RNA, where it plays a pivotal role in enhancing RNA structural stability and modulating its protein interactions.[9]

The integration of Ψ into therapeutic RNA molecules has significantly advanced the field of RNA-based therapeutics. As such, a landmark 2005 study by Karikó et al. showed that replacing U with Ψ in *in vitro*-transcribed mRNA completely suppressed the pro-inflammatory response from RNA-sensing TLRs.[10] This discovery represented a significant leap forward, especially considering earlier findings that unmodified mRNAs elicited strong immunostimulatory effects, thereby limiting the practicality of mRNA-based transgene expression.[11] Follow-up studies confirmed these findings and demonstrated the superior translation efficiency of Ψ-modified RNA *in vivo*, which was inversely correlated to its immune-stimulatory capacity.[12,13] Further studies in cells devoid of functional TLR signaling documented enhanced translation of Ψ-modified mRNA. This could be attributed to the fact that pseudouridinylated RNA did not trigger PKR activation and thus translational arrest, which was readily observed when using unmodified RNA.[14] Further, Ψ-RNA's failure to activate the OAS RNase L system—an antiviral pathway triggered by unmodified RNA that shuts down translation—also enhanced mRNA translation.[15]

Subsequent studies showed that N1-methylpseudouridine ($m^1\Psi$) enhances translation compared with Ψ-modified mRNA *in vitro* and *in vivo*, partly due to reduced TLR3 stimulation.[16] Unlike Ψ, $m^1\Psi$ is extremely rare in eukaryotes, with only one known site in human 18S rRNA.[17,18] $m^1\Psi$-modified mRNA also showed improved translation in cell-free systems,[19] attributed to suppression of immune/PKR-mediated translation inhibition and alterations in translation dynamics, including increased ribosome pausing and density. These effects were linked to enhanced mRNA stability via secondary structure stabilization.[20] Although extensive direct comparisons between Ψ and $m^1\Psi$ were not made, $m^1\Psi$ was rapidly adopted to suppress innate immune activation and boost mRNA translation.

Given the profound effects of both Ψ and $m^1\Psi$ on RNA stability, translation efficiency, and immunogenicity, it remains challenging to disentangle the individual contributions of these factors. However, there is substantial evidence that TLR7-dependent recognition of unmodified RNA predominantly dictates the pro-inflammatory activity and immunogenicity of mRNA-based vaccines in mice *in vivo*.[21–23] In this context, it has to be noted that TLR8 is not functional in mice and hence not accounted for in such studies. At the same time, it has also been shown that the antiviral responses induced by mRNA therapeutics can adversely affect RNA-driven transgene expression.[24,25]

Interestingly, despite their widespread implementation in mRNA vaccine technologies and other RNA-based therapeutics, the exact mechanisms by which Ψ or $m^1\Psi$ evade immune recognition by the endolysosomal TLR system are unclear. Therefore, we wanted to revisit this unresolved issue, also in light of the recently discovered importance of nuclease activity upstream of TLR7 and TLR8.

RESULTS

A quantitative, mass spectrometry-based approach to analyze RNase T2 cleavage fragments

In previous work, we had employed MALDI-TOF mass spectrometry (MS) as a qualitative MS technology to characterize the cleavage products of RNase T2 using various RNA oligo substrates. Doing so, we had inferred that RNase T2 preferentially cleaves between R and U bases to render fragments that are terminated with a 3′ R and initiated with a 5′ U. Opposed to our initial finding that ssRNA, but not double-stranded RNA (dsRNA), served as a good substrate for RNase T2 (see Greulich et al.[7] and Figure S1A), it was reported that RNase T2 can also degrade dsRNA.[26] Therefore, we wished to revisit this topic and designed 4 oligonucleotides, all of which enable the formation of a hairpin secondary structure (Figures S1B–S1E). While RNase T2 was largely unable to cut hairpin 1, which lacks Us (Figure S1B), and hairpin 2, which contains a GU cleavage site within the stem region (Figure S1C), it efficiently cleaved the RNA when a GU cleavage site was positioned directly in the single-stranded loop region of the hairpin (Figure S1D). Interestingly, when the U in the stem loop was additionally paired with G, forming a non-canonical wobble base pair adjacent to the GU cleavage site, RNase T2 efficiently cut the RNA at the two highest concentrations tested (Figure S1E). RNase 1 on the other side, a member of the RNase A family, was able to cut all 4 hairpin RNAs equally well (Figures S1B–S1E). This data indicates that RNase T2 preferentially cuts non-base-paired RNA. To analyze RNase T2 cleavage products using a more quantitative approach, we digested the previously established model substrate RNA40 under undercutting conditions with RNase T2 (Figure 1A) and analyzed the so-obtained cleavage products using liquid chromatography-MS (LC-MS). We detected 17 distinct RNA fragments (Figure 1B). Due to the presence of well distinguishable, non-overlapping high-performance liquid chromatography (HPLC) peaks in the UV chromatogram, we could determine the abundance of these fragments based on their UV absorbance and extinction coefficient. Relating the amount of the individual fragments to their position in the RNA oligo educt strand showed that we were able to accurately reconstruct all fragments with a decisive abundance. Indeed, when we quantified the abundance of all nucleotides of the educt RNA40 and compared the values with the quantities determined in the identified fragments, we observed an even representation with only a small underrepresentation of position 10–20 of the educt oligo RNA40 (Figure 1C). Based on these data, we could identify three major cut sites, all consisting of a GU dinucleotide. At these sites, 64% (position 5/6), 43% (position 9/10), or 37% (position 12/13) of the RNA40 starting material was cleaved. Only two minor non-GU cleavage events were detected, with 2% at the CU

Please cite this article in press as: Bérouti et al., Pseudouridine RNA avoids immune detection through impaired endolysosomal processing and TLR engagement, Cell (2025), https://doi.org/10.1016/j.cell.2025.05.032

CellPress
OPEN ACCESS

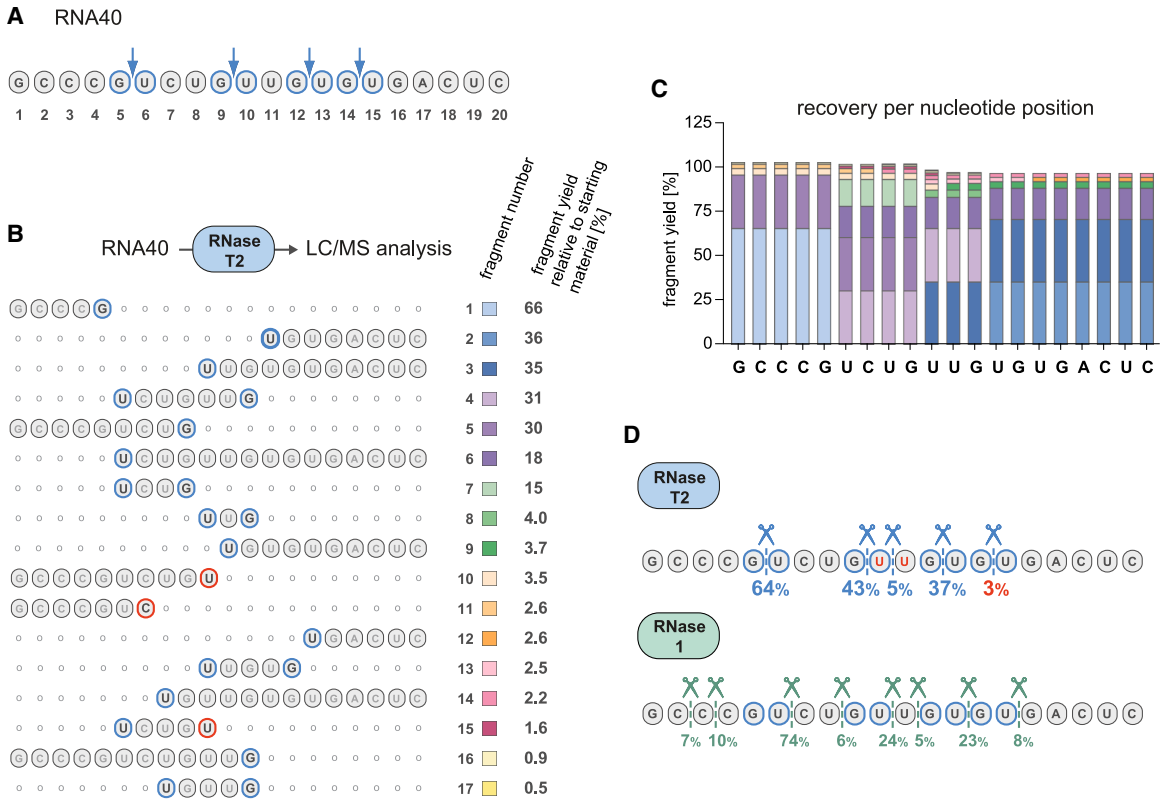

E coverage of dinucleotide sequence motivs as potential cleavage sites

RNA40	BASE2 C	U	G	A
BASE1 C	2	2	1	0
U	1	1	4	0
G	0	4	0	1
A	1	0	0	0

F average cleavage by RNase T2 [%]

RNA40	BASE2 C	U	G	A
BASE1 C	0 < 0.1	1 +/- 1.3	0 –	
U	0 –	5 –	0 < 0.1	
G		37 +/- 22		0 –
A	0 –			

average cleavage by RNase 1 [%]

RNA40	BASE2 C	U	G	A
BASE1 C	9 +/- 1.4	1 +/- 0.7	2 ---	
U	74 –	24 –	10 +/- 7	
G		0 < 0.1		0 –
A	0 –			

G combined coverage of dinucleotide sequence motifs as potential cleavage sites in RNA40, RNA40i and RNA9.2s

RNA40 RNA40i RNA9.2s	BASE2 C	U	G	A
BASE1 C	6	7	1	2
U	4	4	5	5
G	2	5	0	1
A	2	4	1	1

H average cleavage by RNase T2 [%]

RNA40 RNA40i RNA9.2s	BASE2 C	U	G	A
BASE1 C	0 +/- 0.2	6 +/- 12	0 ---	0 +/- 0.1
U	0 < 0.1	5 +/- 5	0 +/- 0.6	1 +/- 0.9
G	0 < 0.1	39 +/- 20		0 ---
A	0 +/- 0.5	36 +/- 19	0 ---	2 ---

average cleavage by RNase 1 [%]

RNA40 RNA40i RNA9.2s	BASE2 C	U	G	A
BASE1 C	11 +/- 12	1 +/- 2	2 ---	22 +/- 18
U	31 +/- 28	6 +/- 10	9 +/- 7	47 +/- 14
G	0 < 0.1	0 < 0.1		0 ---
A	0 < 0.1	1 +/- 0.6	0 ---	0 ---

(legend on next page)

Please cite this article in press as: Bérouti et al., Pseudouridine RNA avoids immune detection through impaired endolysosomal processing and TLR engagement, Cell (2025), https://doi.org/10.1016/j.cell.2025.05.032

position 7/8% and 5% at the UU position 10/11 (Figures 1D, blue color, 1E and 1F, blue color). Using recombinant RNase 1 resulted in a different outcome: now all cleavage sites consisted of a pyrimidine followed by a random nucleotide (YN) (Figures 1D, green color, 1E and 1F, green color). To extend the targeting space of these enzymes we continued our study with the oligonucleotide RNA40i, in which all R bases of RNA40 were inverted (Figure S2A). Subjecting this oligonucleotide to RNase T2 digestion allowed us to identify four major cleavage sites that were all within an AU sequence (Figures S2B–S2D). Interestingly, for this oligonucleotide, the observed cleavage frequencies at the different positions were slightly different, with the second RU site now being the most frequently processed site. Also, no cuts beyond AU were recorded with a frequency higher than 3%. As for RNA40, digestion of RNA40i with RNase 1 resulted in fragments that were all terminated by a pyrimidine (Figures S2B–S2D). Finally, we studied the cleavage of RNA9.2s, another RNA oligo that is commonly used to activate TLR7 or TLR8 (Figure S2E). While the predominant RNase T2 cleavage site within RNA9.2s was again the central GU motif (position 11/12) with 50% processing at this side, also two additional non-RU cleavage sites were found with 14% cleavage at UU (position 4/5) and 34% at CU (position 9/10). RNase 1 dependent processing of RNA9.2s again provided only pyrimidine-terminated fragments (Figures S2E–S2G). Combining the processing data of all three oligonucleotides confirmed that RU dinucleotides are the optimal cleavage site for RNase T2. RNase 1, on the other hand, cleaves atYN with a preference for either YC or YA (Figures 1G and 1H).

RNase T2 substrate specificity for complex RNA molecules

In light of the notion that we observed the cleavage of non-RU substrates by RNase T2 under certain conditions, we wished to explore the substrate specificity of RNase T2 and RNase 1 on a complex RNA molecule, hence mimicking a physiological substrate. To do so, we *in vitro* transcribed a 2,500-nt ssRNA molecule and subjected this RNA to RNase T2 and RNase 1 digestion. Using LC-MS, we detected masses in the analyzed LC elution window, which encompassed dimers and trimers (Figure 2A). As expected, the UV chromatograms as well as the MS signal intensities were clearly distinct for these two treatments. Due to the complexity of the UV chromatograms with several peaks overlapping, we could not quantify the abundance of individual fragments by UV absorption. However, we could use the MS signal intensities of the fragments obtained by RNase T2 and RNase 1 digestion to calculate a ratio for a given fragment between the two samples, using the condition with the higher abundance as the reference (Figures 2B and 2C). Conducting this analysis revealed that dinucleotides UA and UG were exclusively seen for RNase T2, whereas their isomers AU and GU were only seen when digesting the RNA with RNase 1. Also, the other pyrimidine-terminated dinucleotides such as CU, UC, GC, AC, and CC as well as UU were either exclusively or predominantly observed when digesting the RNA molecule with RNase 1. Consistent with their substrate specificity, R-terminated dinucleotides that were not initiated by U (CG, CA, GA, AG, GG, and AA) were only detected at low abundance or trace amounts for both RNase T2 and RNase 1 digestion. Extending this analysis to certain trinucleotides confirmed this picture. U-initiated, R-terminated trinucleotides such as UUG or UUA were exclusively seen in RNase T2 digested samples, whereas their isomers were either confined to the RNase 1-treated sample (UGU, GUU, or AUU) or only detected at low abundance (UAU). Altogether, in a setting in which all possible dinucleotide substrates are available, RNase T2 preferentially cleaves substrates at RU, whereas RNase 1 cleaves after pyrimidine. Thus, it can be concluded that cleavage of non-RU substrates by RNase T2 is only observed under conditions of a restricted target range.

RNase T2 shows strongly reduced activity toward Ψ RNA

Next, we wanted to investigate whether modifications that occur naturally in RNA molecules affect the activity of RNase T2. To do this in a more reductionist setting, we used a previously established oligonucleotide containing a defined RNase T2 cleavage site. The used substrate consists of a stretch of 14 deoxynucleotides followed by a 6-nt RNA motif (UUGUCU) with a central GU dinucleotide (Figure 3A). Transferase-type ribonucleases, such as RNase T2 and RNase 1, cleave their substrates by catalyzing a 2′-O-transphosphorylation step that yields a cyclic 2′,3′-phosphodiester product of the fragment 5′ of the scissile bond and the concomitant release of a 5′OH fragment 3′ of the

Figure 1. Characterization of ssRNA digested with RNase T2 or RNase 1

(A) Scheme of RNA40 and its major RNase T2 cut sites.

(B) RNA40 (1 μg) was digested with RNase T2 (35 nM) in IDTE buffer and analyzed by HPLC-HESI-MS. The molecular identity and the fragment yields of the 17 identified fragments generated by RNase T2 digestion of RNA40 are shown. Fragment yields (percent product of educt) from three independent experiments were summarized.

(C) The yield of the fragments identified in (B) is shown for each nucleotide position.

(D) The percentage of cleavage at a given site for RNA40 processed by RNase T2 (35 nM) or RNase 1 (3 nM) is indicated. All sites with >3% cleavage are shown; RNase T2 cleavage percentage for the fourth GU motif is also depicted. Data from three independent experiments were summarized.

(E) The coverage of dinucleotide motifs as potential cleavage sites in RNA40 is shown. Note that only internal sites are considered, as RNase T2 and RNase 1 do not have exonuclease activity.

(F) Average cleavage percentages for all possible dinucleotide motifs of RNA40 digested with RNase T2 (35 nM) or RNase 1 (3 nM). Data from three independent experiments were summarized and cleavage percentages are depicted as mean values (large letters) ± SD (small letters, below).

(G) The coverage of dinucleotide motifs as potential cleavage sites in RNA40, RNA40i, and RNA9.2s are shown (only internal sites considered).

(H) Average cleavage percentages for all possible dinucleotide motifs of RNA40, RNA40i, and RNA9.2s digested with RNase T2 or RNase 1 were calculated from (F) and Figures S2D and S2G by summing the individual cleavage percentages of a given dinucleotide motif divided by the number of occurrences of that cleavage site in all three oligonucleotides. Data are depicted as mean values ± SD.

See also Figures S1 and S2.

Please cite this article in press as: Bérouti et al., Pseudouridine RNA avoids immune detection through impaired endolysosomal processing and TLR engagement, Cell (2025), https://doi.org/10.1016/j.cell.2025.05.032

CellPress
OPEN ACCESS

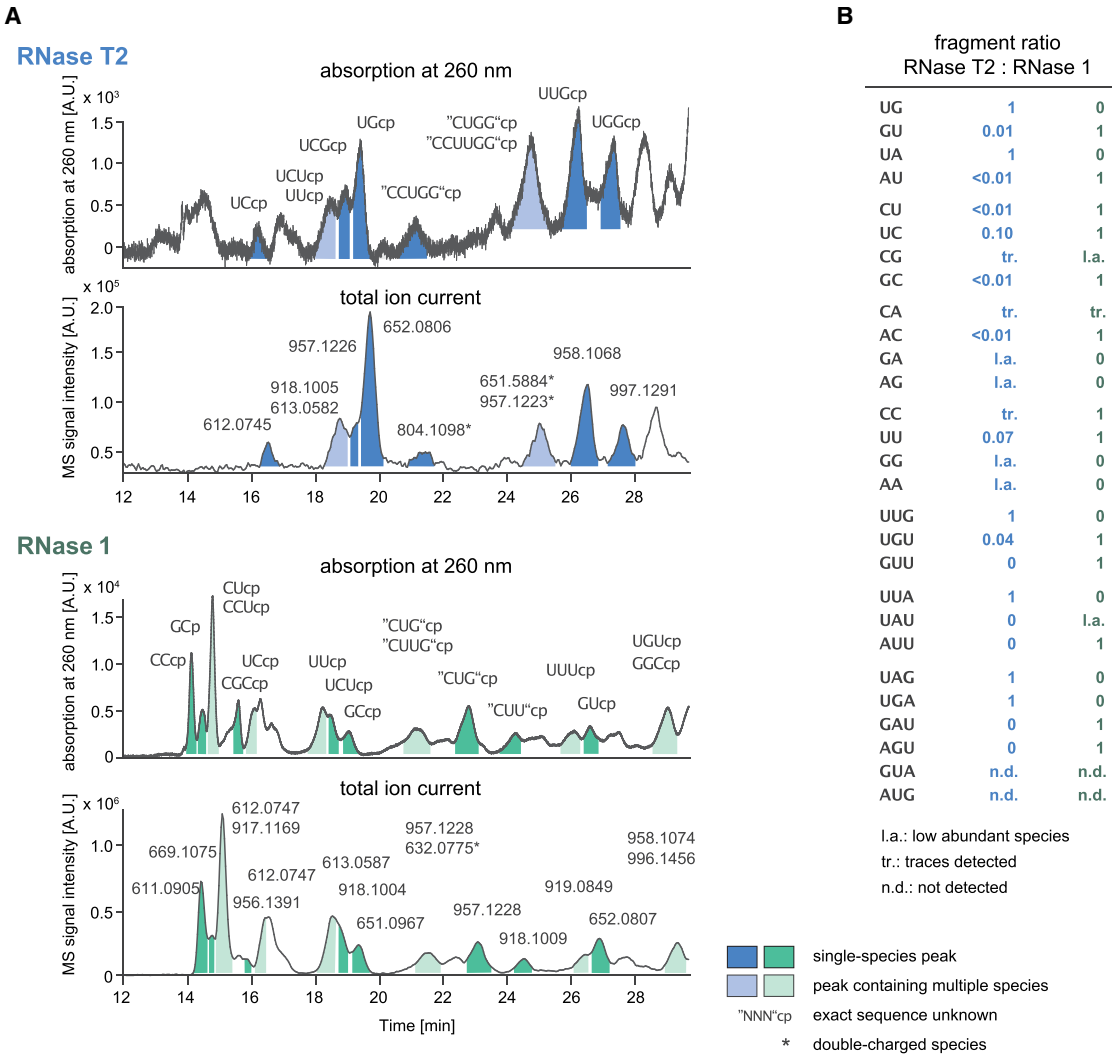

(legend on next page)

Please cite this article in press as: Bérouti et al., Pseudouridine RNA avoids immune detection through impaired endolysosomal processing and TLR engagement, Cell (2025), https://doi.org/10.1016/j.cell.2025.05.032

scissile bond. This step requires a free 2′OH group of the nucleotide at the B1 position (Figure 3B). Consistent with this notion, replacement of the G of UUGUCU with a 2′-O-methylguanosine (UUGmUCU) indeed largely abolished RNase T2-dependent cleavage of this oligonucleotide (Figures 3C and 3D). In contrast, 2′-O-methylation of the U in this motif (UUGUmCU) had no effect on RNase T2-dependent cleavage of this oligo, consistent with its cleavage mechanism (Figures 3C and 3D). Mass spectrometric analysis of the cleaved fragments confirmed these results (Figure 3E, left). While the GU-containing oligonucleotide was cleaved preferentially between G and U by RNase T2, this activity was fully abolished by the introduction of a 2′-O-methylguanosine. Of note, RNase 1 cleaved this oligo preferentially after the U at position 1 and position 4 of the 6-nt RNA motif (Figure 3E, right), whereas the introduction of a 2′-O-methylguanosine had no effect on this selectivity.

Next, we investigated whether Ψ or $m^1Ψ$ instead of U would affect RNase T2 activity (Figure 3C). We introduced Ψ or $m^1Ψ$ into the B2 position of the RNase T2 dinucleotide motif. Interestingly, neither GΨ nor $Gm^1Ψ$ were cleaved by RNase T2 as shown by PAGE and LC-MS analysis (Figures 3F and 3G, left). Since Ψ or $m^1Ψ$ was also part of the second cleavage site of the oligo preferentially cleaved by RNase 1, we could also assess the effect of this modification on RNase 1 activity. This revealed that RNase 1 in contrast to RNase T2 processed Ψ or $m^1Ψ$ just like U (Figure 3G, right). Since RNase 2 and RNase 6 have also been reported to act upstream of TLR8,[26,27] we included these RNase A family members in our analysis. As shown above, RNase T2 was largely unable to cleave between GΨ, while RNase 2 and RNase 6, similar to RNase 1, processed Ψ to a comparable extent as U (Figure 3H). Building on these findings, we also tested RNase T2 activity on a long, complex ssRNA substrate by transcribing the previously used 2,500-nt template *in vitro*, incorporating either U, Ψ, or $m^1Ψ$. Incubation of these RNAs with RNase T2 revealed that Ψ- and $m^1Ψ$-containing RNAs remained largely intact at low enzyme concentrations (Figure 3I, +), whereas U-containing RNA was completely digested. At higher enzyme concentrations (Figure 3I, ++), modified RNA substrates were also degraded by RNase T2 but to a lesser extent than unmodified RNA. These results suggest that RNase T2 cannot accommodate 2′-O-methylated Rs in its B1 pocket, as it requires a free hydroxyl group at this position. Furthermore, the B2 pocket of RNase T2 disfavors Ψ and $m^1Ψ$. In contrast, RNase A family members process Ψ and $m^1Ψ$ similarly to U.

Ψ RNA does not activate TLR8

In the next step, we evaluated the immune-stimulatory potential of these long ssRNA substrates in primary human monocytes in the presence of the TLR8-specific inhibitor CU-CPT9a. As expected, Ψ- or $m^1Ψ$-containing *in vitro* transcripts (IVTs) failed to stimulate TLR8 in primary human monocytes, while the unmodified IVT clearly triggered a TLR8-dependent interleukin-6 (IL-6), interferon gamma-induced protein 10 (IP-10), and tumor necrosis factor (TNF) response (Figures 4A–4C). Similar results were obtained in primary human peripheral blood mononuclear cells (PBMCs) (Figure S3A) and the monocytic cell line THP-1 (Figure S3B). We further utilized the BLaER1 monocyte model as these cells have been shown to respond to ssRNA when delivered with the cationic polypeptide poly-L-arginine (pR) in a TLR8- and RNase T2-dependent manner.[7] Like for primary human cells, the unmodified IVT induced a TLR8- and RNase T2-dependent IL-6 response in BLaER1 monocytes, while Ψ- or $m^1Ψ$-containing IVTs failed to stimulate TLR8 (Figure 4D). To exclude the possibility that uptake accounts for the differences observed, we transfected BLaER1 monocytes with fluorescently labeled RNAs and monitored their uptake by fluorescence-activated cell sorting (FACS). These data indicate that the RNA is equally taken up by cells independent of the RNA modification present (Figure S3C). At the same time, varying the oligonucleotide length did not affect the immune-stimulatory activity of IVT-U RNA, while Ψ-containing IVTs of any length failed to induce TLR-dependent interferon (IFN) release in PBMCs (Figure S3D). To study the impact of pseudouridylation in a setting in which a single RNase T2 motif is affected, we also tested the different UUGUCU-containing oligonucleotides (Figure 3) for their biological activity (Figure 4E). At the concentrations tested, the unmodified $(dAdC)_7$-UUGUCU oligonucleotide induced similar levels of IL-6 as RNA40. This activity was dependent on both RNase T2 and TLR8. All other oligonucleotides tested showed no TLR8 agonistic activity. These results are fully consistent with the observation that the GmU-, GΨ-, and $Gm^1Ψ$-containing oligonucleotides are no longer cleaved by RNase T2 (Figures 3D and 3F). Interestingly, the GUm-containing oligonucleotide was no longer stimulatory despite being cleaved by RNase T2 (Figure 3D). We speculate that this is due to reduced lysosomal U release, consistent with previous findings showing that the 3′-terminal fragment UCU is critical for this effect.[7] To further investigate this, we tested whether RNase A enzymes can cleave 2′-O-methyl Us, as RNase 2—a member of this family—has been implicated in U release for pocket 1.[26] As expected, based on their mode of action, none of these enzymes were able to cleave 2′-O-methyl Us (Figures S3E–S3G). Similarly, the lysosomal exonucleases PLD3 and PLD4 exhibited reduced activity but were not entirely inactive toward 2′-O-methyluridine-containing substrates (Figures S3H and S3I). In summary, these results indicate that Ψ-containing RNA fails to activate TLR8 across a wide range

Figure 2. Characterization of RNase T2 or RNase 1 digestion of a complex RNA substrate

(A) A 2,500 nt IVT (1 μg) was digested with RNase T2 (3.5 μM) or RNase 1 (3 nM). Representative LC-UV and LC-MS chromatograms of the two digests are shown (only the elution window from 12–30 min is shown). Annotated are fragment sequences with their corresponding masses (i.e., *m/z* values) as identified by LC-MS. The chromatograms are representative for two (RNase T2) or three (RNase 1) independent experiments.

(B) Ratios of different fragments (all with 2′,3′-cyclic monophosphate moiety at the 3′ end) present in the RNase T2 and/or RNase 1 digest as found by LC-MS. The fragment ratios are representative for two or three independent measurements. Note that the nonbinary results can only be considered as estimates, since no internal standards were available.

(C) Comparison of exemplary fragments of a specific mass/overall nucleotide composition as found by LC-MS in digests with the two enzymes. The resulting MS peaks correspond to specific fragment sequences. Data represent two or three independent experiments.

Please cite this article in press as: Bérouti et al., Pseudouridine RNA avoids immune detection through impaired endolysosomal processing and TLR engagement, Cell (2025), https://doi.org/10.1016/j.cell.2025.05.032

CellPress
OPEN ACCESS

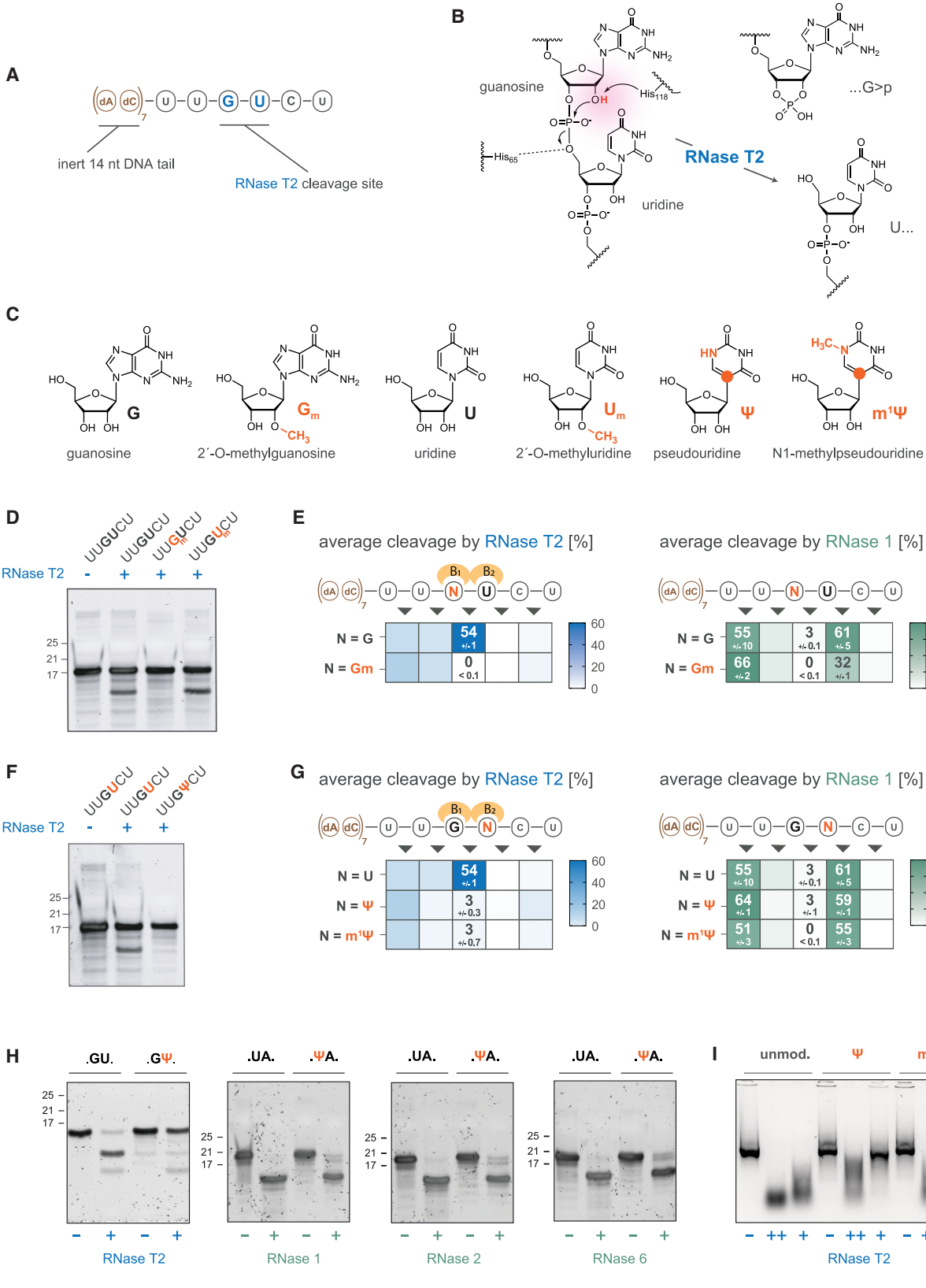

(legend on next page)

Please cite this article in press as: Bérouti et al., Pseudouridine RNA avoids immune detection through impaired endolysosomal processing and TLR engagement, Cell (2025), https://doi.org/10.1016/j.cell.2025.05.032

of cell types. In a reductionist setting, this lack of immunogenicity can be attributed to the modification affecting a single RNase T2 cleavage site.

Ψ is not a ligand for TLR8

Our results suggested that RNase T2 no longer generates RNA fragments from Ψ- or $m^1Ψ$-modified RNA, which was previously identified as a critical upstream requirement for TLR8 activation. However, these results could not exclude that Ψ or $m^1Ψ$ single nucleosides are still released from ssRNA, e.g., by RNase A enzymes in cells, and that the observed lack of immune stimulation is primarily due to these molecules not acting as agonists for TLR8. Under physiological conditions, RNA fragments engage the second binding pocket to allosterically regulate U binding in the first pocket, whereas small-molecule agonists such as R848 or TL8 bypass this requirement.[4] Binding studies indicate that TLR8 can bind U independently of the second pocket, albeit with a >50-fold reduction in affinity. Based on these considerations, we hypothesized that it should be possible to stimulate TLR8 in cells by hyperphysiological concentrations of U alone (Figure 5A). Indeed, at up to 32 mM, U elicited an IL-6 response of similar efficacy as TL8 but with greatly reduced potency (EC_{50} for TL8, 128 nM[28]; EC_{50} for U, 10.7 mM) (Figures S3J and S3K). Comparing U, Ψ, or $m^1Ψ$ as a pocket one agonist in cell culture, we again determined a high TLR8 agonistic efficacy for U (top IL-6 levels at 167.2 ng/ml) with an EC_{50} of 9.3 mM. Ψ, however, was completely inactive in stimulating TLR8 in the range tested (4–32 mM). Interestingly, $m^1Ψ$ induced a significant IL-6 response, albeit with reduced efficacy compared with U (IL-6 levels at 72.1 ng/ml), yet with a comparable EC_{50} (9.9 mM) (Figure 5B). Analogous results were obtained using primary monocytes (Figure S3L). Since 2′-O-methylation only partially inhibits PLD exonucleases, we tested whether 2′-O-methyluridine could activate TLR8. Here, like Ψ, 2′-O-methyluridine was unable to activate TLR8 in cells (Figure S3M). Next, we investigated whether U, Ψ, and $m^1Ψ$, when co-delivered with ssRNA, could enhance the TLR8-dependent RNA response. Therefore, we stimulated BLaER1 monocytes with $ssRNA40^S$ and the three single nucleosides (1.25–5 mM). U increased the RNA response by ~3-fold, with a similar effect observed for $m^1Ψ$ (Figures 5C and 5D). Surprisingly, Ψ, despite not inducing TLR8 activation alone (Figure 5B), enhanced the RNA response ~2-fold (Figure 5D), suggesting potential TLR8 binding. A similar effect was observed for 2′-O-methyluridine with $ssRNA40^S$ (Figure S3N).

Our results suggested that Ψ and $m^1Ψ$ can bind TLR8 when released from ssRNA, though Ψ is a weaker substrate than U and $m^1Ψ$. Despite their similar uptake, we aimed to investigate direct TLR8 stimulation through a biochemical assay that measures ligand-induced dimerization (Figure 5E). Unlike binding assays, this method distinguishes agonists from competitive antagonists. We expressed and purified human TLR8 ectodomain (ECD), confirming its autoprocessing at the Z-loop (Figure S4A) and its 110 kDa size at pH 5.0 via mass photometry (Figure S4B). Incubation with U (0.625–5 mM) revealed a dose-dependent ECD dimerization, reaching ~60% at 5 mM U (Figure 5F, left). Ψ showed minimal dimerization, even at the highest concentration (Figure 5F, middle), while $m^1Ψ$ mirrored U's activity (Figure 5F, right). In contrast, 2′-O-methyluridine failed to induce dimerization (Figure S4C). We further co-incubated the single nucleosides with $ssRNA40^O$ to introduce a second binding pocket ligand (Figures 5E and 5F, bottom row). While $ssRNA40^O$ alone failed to induce TLR8 ECD dimerization *in vitro* (Figure S4D), its combination with U or $m^1Ψ$ further enhanced dimer formation compared with the nucleosides alone (Figure 5F, bottom left and right). Notably, although $ssRNA40^O$ and Ψ individually showed little to no dimerization, their combination triggered robust dimerization, albeit weaker than U + ssRNA or $m^1Ψ$ + ssRNA (Figure 5F, bottom middle), aligning with stimulation results. In contrast, ssRNA with 2′-O-methyluridine induced the weakest dimerization (Figure S4E), suggesting the lowest TLR8 binding affinity among the tested nucleosides. Last, to rule out the competitive binding of Ψ to TLR8, we stimulated BLaER1 monocytes with U alone or combined with increasing Ψ concentrations. Co-stimulation did not reduce the U-dependent TLR8 response (Figure S4F). Taken together, these results indicate that Ψ as well as Um are much weaker substrates for TLR8 compared with U, however binding is not completely prohibited. Surprisingly, $m^1Ψ$ exhibits similar TLR8 activation to U.

Ψ inhibits the release of 2′,3′-cGMP for TLR7 activation

Beyond its lack of TLR8 stimulation, Ψ RNA also strongly dampens the TLR7 response.[10] In line with this notion, IVT-Ψ and IVT-$m^1Ψ$

Figure 3. Ψ and $m^1Ψ$ impair RNA cleavage by RNase T2 but not RNase A enzymes

(A) Chimeric DNA-RNA oligonucleotides used as test substrate for cleavage experiments with RNase T2 and RNase 1.

(B) RNA cleavage mechanism of a transferase-type endoribonuclease exemplified on a GU dinucleotide site.

(C) Structures of guanosine, 2′-O-methylguanosine, uridine, 2′-O-methyluridine, Ψ, and $m^1Ψ$.

(D) Indicated oligonucleotides (1 μg each) were subjected to RNase T2 (9 μM) cleavage in IDTE buffer and analyzed on a denaturing urea gel. Data represent two independent experiments.

(E) HPLC-HESI-MS analysis of cleavage by RNase T2 (3.5 μM) and RNase 1 (6 nM) in IDTE buffer using oligonucleotides (1 μg each) with either guanosine or 2′-O-methylguanosine. Mean cleavage percentages ± SD from three independent experiments.

(F) Unmodified or modified oligonucleotides (1 μg each) were subjected to RNase T2 (9 μM) cleavage in IDTE buffer and analyzed on a denaturing urea gel. Data represent two independent experiments.

(G) Cleavage by RNase T2 (3.5 μM) and RNase 1 (6 nM) on oligonucleotides (1 μg) with U, Ψ, or $m^1Ψ$, analyzed by HPLC-HESI-MS. Mean cleavage percentage ± SD from three independent experiments.

(H) Urea gel of $(dAdC)_7$UUGUCU and $(dAdC)_7$UUGΨCU digested with RNase T2 (10 nM) in assay buffer. One representative blot of three independent experiments is shown. Urea gels of $(dAdC)_7$GAGUAGA and $(dAdC)_7$GAGΨAGA digested with RNase 1 (60 nM), RNase 2 (55 nM), or RNase 6 (60 nM) in assay buffer. One representative blot of two independent experiments.

(I) IVTs containing U, Ψ, or $m^1Ψ$ were digested with RNase T2 (+ = 0.37 μM) and (++ = 3.7 μM) for 20 min and analyzed on a non-denaturing agarose gel. Data represent two independent experiments.

Please cite this article in press as: Bérouti et al., Pseudouridine RNA avoids immune detection through impaired endolysosomal processing and TLR engagement, Cell (2025), https://doi.org/10.1016/j.cell.2025.05.032

CellPress
OPEN ACCESS

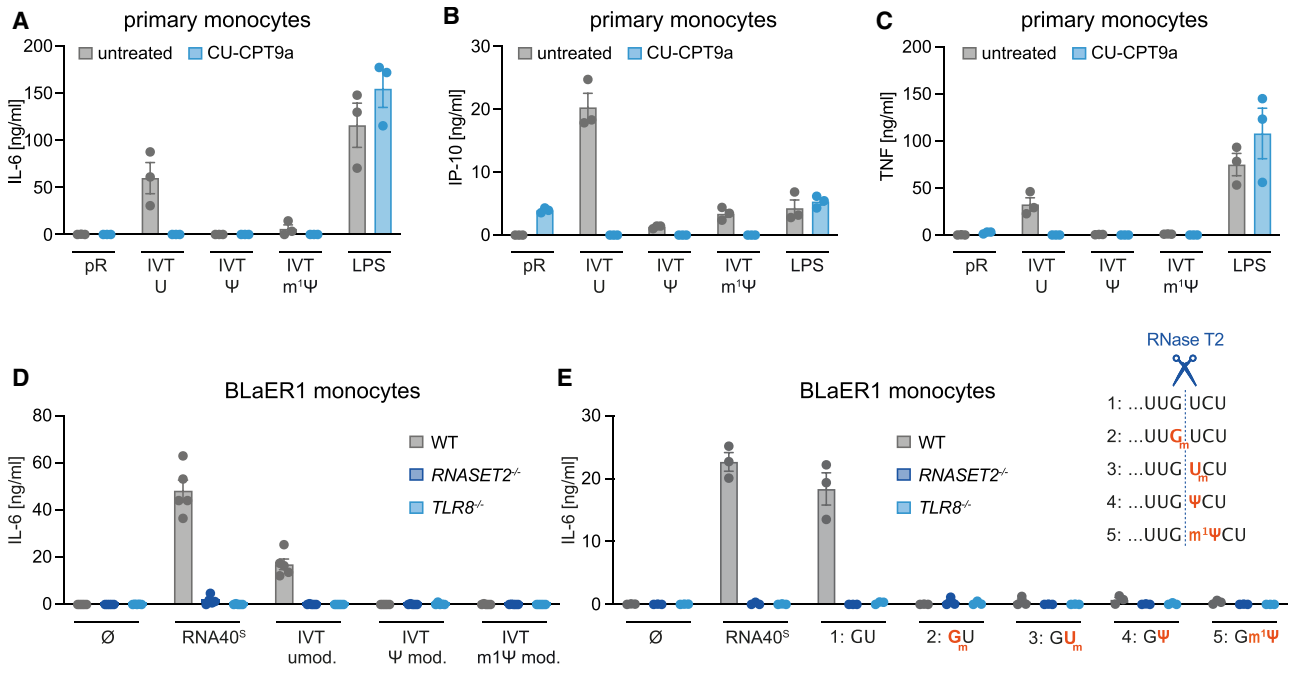

Figure 4. Ψ RNA does not activate TLR8

(A–C) CD14$^+$ monocytes were stimulated with pR, OVA IVT-U, OVA IVT-Ψ, OVA IVT-m^{1}Ψ, and LPS in the presence or absence of CU-CPT9a. After 24 h, (A) IL-6, (B) IP-10, and (C) TNF release was measured. Data are depicted as mean ± SEM of n = 3 independent donors.

(D) BLaER1 monocytes of indicated genotypes were unstimulated or stimulated with ssRNA40^S, Cas9 IVT-U, Cas9 IVT-Ψ, and Cas9 IVT-m^{1}Ψ. After 14 h, IL-6 release was measured. Mean ± SEM of n = 5 independent experiments.

(E) BLaER1 monocytes of indicated genotypes were stimulated as indicated. After 14 h, IL-6 release was measured. Mean ± SEM of n = 3 independent experiments.

See also Figure S3.

RNA failed to activate TLR7 in primary plasmacytoid dendritic cells (pDCs), whereas IVT-U RNA induced TLR7-dependent IFNα release upon transfection (Figure 6A). Similar but weaker effects were observed when using lipofectamine instead of pR for delivery (Figure S5A). We recently found that RNase T2 and PLD exonucleases are essential for generating stimulatory ssRNA fragments for TLR7. Accordingly, IVT-U mRNA triggered a TLR7-dependent response in CAL-1 cells, which was entirely reliant on these nucleases, whereas Ψ-modified IVTs failed to induce any response (Figure 6B). Specifically, RNase T2 and PLD collaboratively process RNA to generate 2′,3′-cGMP, the endogenous TLR7 pocket 1 ligand. RNase T2 first cleaves ssRNA between G and U, producing 2′,3′-cGMP-terminated fragments, which PLD exonucleases further degrade into single nucleotides, releasing 2′,3′-cGMP (see Bérouti et al.[8]; Figure 6C). Since RNase T2 poorly processes Ψ- and m^{1}Ψ-containing RNAs (Figures 3F and 3G, left), and cleavage at GΨ is crucial for 2′,3′-cGMP release, we hypothesized that Ψ and m^{1}Ψ impair its production. To test this, we digested the IVT constructs with RNase T2, PLD3, or both, and analyzed 2′,3′-cGMP release via LC-MS. As expected, only the RNase T2 + PLD3 combination efficiently released 2′,3′-cGMP from IVT-U RNA, while substitution with Ψ or m^{1}Ψ (IVT-Ψ, IVT-m^{1}Ψ) completely abolished its release (Figure 6D). Consistent with this, we observed 2′,3′-cGMP production in primary pDCs stimulated with IVT-U RNA, whereas IVT-Ψ RNA led to a markedly reduced release (Figures 6E and 6F). We further stimulated CAL-1 cells with RNA40^O, RNA9.2s, and modified RNA9.2s variants. RNA9.2s is ideal for studying RNase T2's impact, as it contains a single GU cleavage site, which should be essential for generating 2′,3′-cGMP. Indeed, blocking RNase T2 cleavage by adding a 2′-O-methylation to G at this site (Figure 3D) completely abolished RNA9.2s's immune-stimulatory effect (Figures 6G and S5B). Similarly, substituting U with Ψ at the cleavage site strongly reduced but did not fully eliminate TLR7 responses. However, adding three additional Ψs upstream of the GU site completely abrogated RNA9.2s's immune-stimulatory potential (Figures 6G and S5B). Intriguingly, these effects correlated with 2′,3′-cGMP release by RNase T2 and PLD3 *in vitro* (Figure 6H). Notably, all oligonucleotides retained a U-containing motif (CCUUC) necessary for TLR7 pocket 2,[6] indicating that the blunted or reduced TLR7 response resulted primarily from impaired 2′,3′-cGMP release. These findings indirectly suggest that PLD exonucleases, like RNase T2, do not efficiently process Ψ as a substrate. Since PLD exonucleases must degrade RNase T2-processed RNA to the single nucleotide level to release 2′,3′-cGMP, we examined whether PLD3 and PLD4 can degrade Ψ and m^{1}Ψ when encountered at the 5′ end. To formally address this, we incubated PLD3 and PLD4 with oligonucleotides starting with three consecutive U, Ψ, or m^{1}Ψ. As expected, both enzymes efficiently degraded U-RNA but failed to effectively digest Ψ- or m^{1}Ψ-RNA (Figures S5C and S5D). Further analysis using PLD3^{H201N,H416N}, a catalytically inactive mutant that retains substrate binding,[8] showed a ∼4-fold reduction in

Please cite this article in press as: Bérouti et al., Pseudouridine RNA avoids immune detection through impaired endolysosomal processing and TLR engagement, Cell (2025), https://doi.org/10.1016/j.cell.2025.05.032

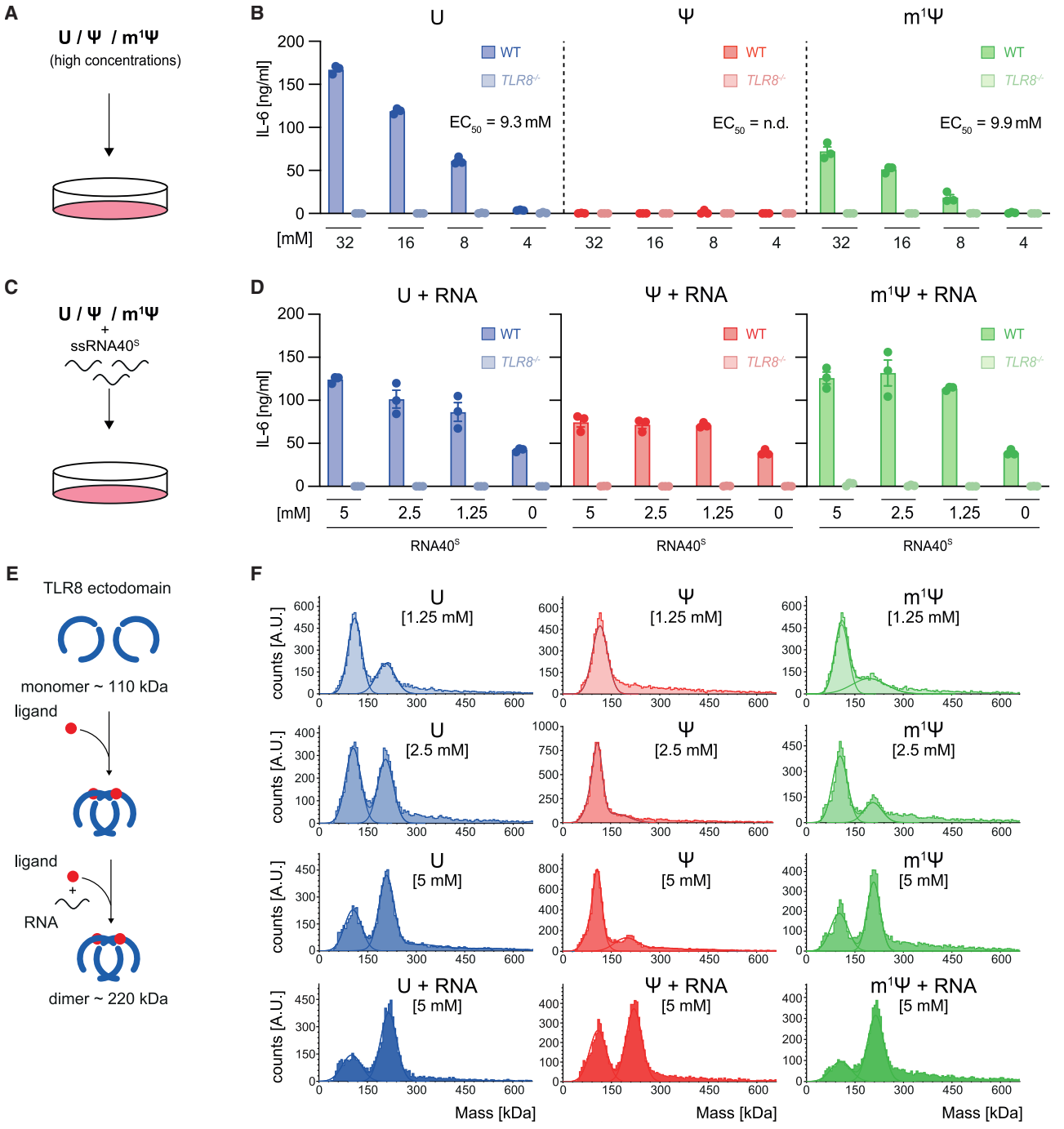

Figure 5. Ψ is a poor ligand for TLR8

(A) Scheme of cell stimulation with high concentration of single nucleosides.

(B) Wild-type and TLR8$^{-/-}$ BLaER1 monocytes were stimulated with indicated concentrations of U, Ψ, or m^{1}Ψ. After 14 h, IL-6 release was detected. Data are depicted as mean ± SEM of $n = 3$ independent experiments. A four-parameter dose-response curve was fitted to calculate half-maximal effective concentration (EC_{50}).

(C) Scheme of cell stimulation with high concentration of single nucleosides in combination with ssRNA40^S.

(D) Wild-type and TLR8$^{-/-}$ BLaER1 monocytes were stimulated with ssRNA40^S or with ssRNA40^S in combination with U (left), Ψ (middle), or m^{1}Ψ (right). After 14 h, IL-6 release was detected. Mean ± SEM of $n = 3$ independent experiments. Please note that the ssRNA40^S-only control data for Ψ and m^{1}Ψ are identical and that one of the U control replicates is also shared with the Ψ/m^{1}Ψ control.

(E) Scheme of the TLR8 ECD dimerization assay.

(F) Mass distribution of hsTLR8 (AA27-827) observed by mass photometry after incubation with increasing concentrations of single nucleosides and in combination with ssRNA40^O.

See also Figures S3 and S4.

Please cite this article in press as: Bérouti et al., Pseudouridine RNA avoids immune detection through impaired endolysosomal processing and TLR engagement, Cell (2025), https://doi.org/10.1016/j.cell.2025.05.032

CellPress
OPEN ACCESS

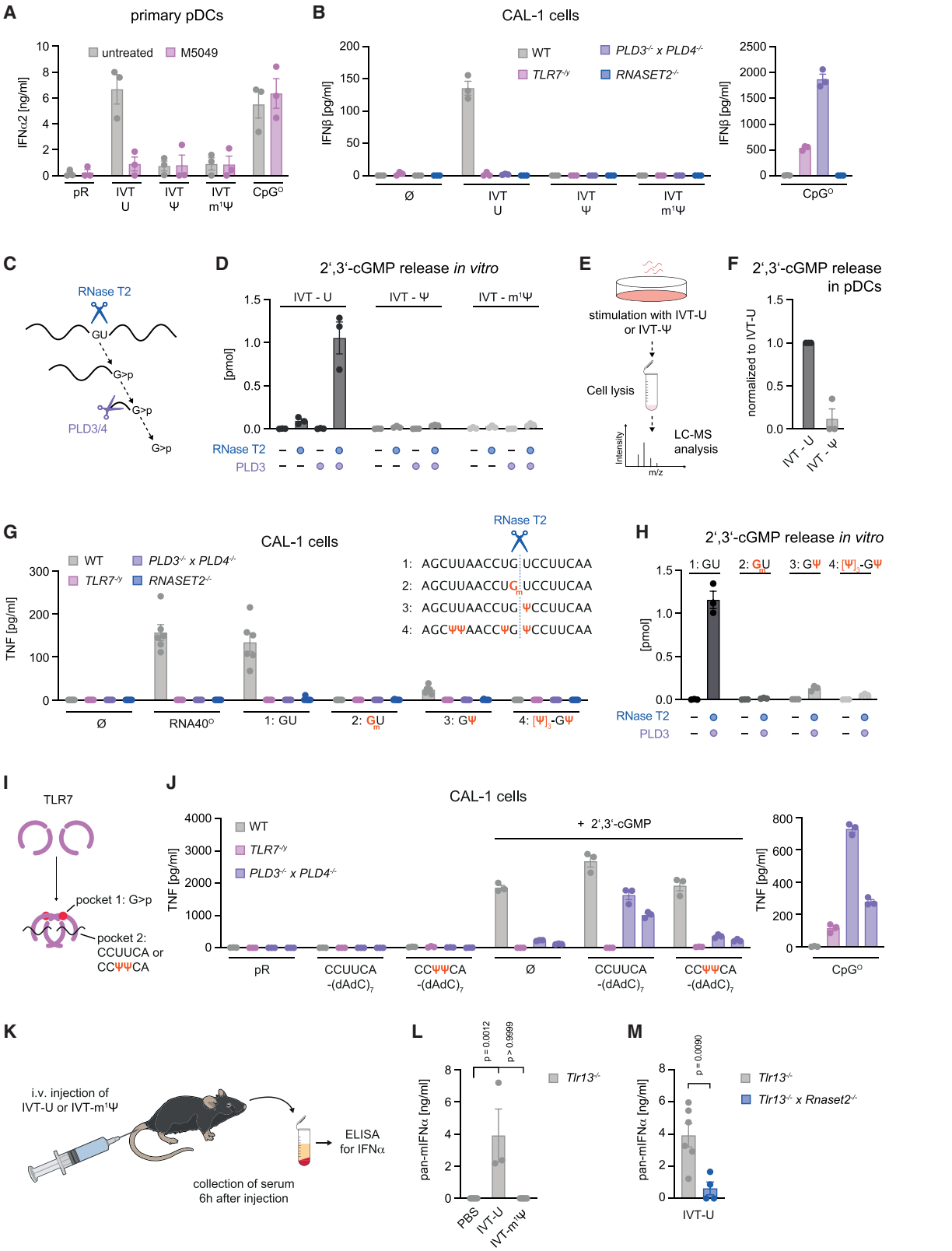

(legend on next page)

Please cite this article in press as: Bérouti et al., Pseudouridine RNA avoids immune detection through impaired endolysosomal processing and TLR engagement, Cell (2025), https://doi.org/10.1016/j.cell.2025.05.032

binding affinity, from 71.38 nM (U-RNA) to 266.3 nM (Ψ-RNA) (Figure S5E). Consistent with previous work,[29] we found that Ψ-containing RNA favors an A-form helical conformation by analyzing Ψ-RNA using NMR. These data indicate additional intramolecular interactions of the Ψ base with the phosphate backbone and Ψ-mediated base stacking between Ψ and the 3′ neighboring base leading to a preferential conformation of the RNA from B into A helical form (Figures S6A–S6D). These structural changes could explain why Ψ is a poor substrate for RNase T2 and PLD exonucleases.

In addition to 2′,3′-cGMP for pocket 1, TLR7 requires a short oligoribonucleotide (ORN) in the second binding pocket, preferably with two consecutive Us for activation.[5] To determine whether Ψ-containing ORNs engage TLR7 pocket 2, we stimulated PLD3xPLD4-deficient CAL-1 cells with 2′,3′-cGMP and a short U- or Ψ-rich oligonucleotide. These cells serve as a model for studying pocket 2 ligands, as they do not respond to the pocket 1 ligand alone (see Bérouti et al.[8]; Figures 6I and 6J), indicating the lack of a pocket 2 ligand under steady state. As expected, co-stimulation with 2′,3′-cGMP and a U-containing oligonucleotide induced TLR7-dependent TNF release. However, when U was replaced with Ψ, no TNF release was observed, suggesting that Ψ cannot allosterically activate TLR7 via the second pocket (Figure 6J). A major challenge of mRNA delivery via LNPs *in vivo* is the low efficiency of endosomal escape, limiting the amount of RNA that reaches the cytosol.[30] As a result, mRNA vaccination triggers a strong TLR7-dependent immune response.[21–23] Since TLR7 drives this response, we hypothesized that it would also depend on RNase T2. However, as RNase T2-deficient mice develop TLR13-driven autoinflammation,[31,32] we investigated mRNA vaccination effects in *Tlr13*$^{-/-}$ × *Rnaset2*$^{-/-}$ double-deficient mice. First, we injected *Tlr13*$^{-/-}$ control mice with IVT-U or IVT-m^{1}Ψ mRNA (Figure 6K). As expected, IVT-U mRNA induced high IFNα levels in the serum, whereas IVT-m^{1}Ψ mRNA did not (Figure 6L). We then compared responses in *Tlr13*$^{-/-}$ and *Tlr13*$^{-/-}$ × *Rnaset2*$^{-/-}$ mice after IVT-U mRNA injection. While *Tlr13*$^{-/-}$ mice showed elevated IFNα levels, IFNα production was significantly reduced in *Tlr13*$^{-/-}$ × *Rnaset2*$^{-/-}$ mice (Figure 6M), demonstrating that RNase T2 is crucial for mRNA recognition *in vivo*. In summary, these results not only show that Ψ as well as m^{1}Ψ impair the release of 2′,3′-cGMP required for TLR7 pocket 1 by inhibiting efficient degradation by RNase T2 and PLD exonucleases, but also that Ψ does not serve as a ligand for the second binding pocket of TLR7.

DISCUSSION

In this study, we investigated how Ψ, the most abundant modification in endogenous RNA, and m^{1}Ψ, the U analog used in prophylactic COVID-19 vaccines, evade recognition by the endolysosomal TLR system. We began by revisiting RNase T2 substrate specificity, as prior reports suggested it was more relaxed, with limited B1 site selectivity for Rs.[26,33] Using quantitative MS, we confirmed our earlier findings that RNase T2 strongly prefers RU motifs. While YU cuts also occurred in a model substrate, they were less frequent. As expected, RNase 1, an enzyme of the RNase A family, cleaved substrates following pyrimidines. Extending these studies to complex RNA substrates—long *in vitro* transcripts—we found that R-terminated fragments were almost exclusively generated by RNase T2. Thus, in a setting with diverse potential substrates, RNase T2 favors RU motifs, whereas in limited substrate contexts, it may act more broadly. Given RNase T2's critical role in processing RNA upstream of TLR7 and TLR8, we reasoned that modifications within RU motifs might regulate TLR activation. Consistent with its catalytic mechanism involving 2′-O-transphosphorylation of the first nucleotide, we found that 2′-O-methylation of G—but not U as the second nucleotide—completely blocked GU cleavage by RNase T2.[33] Turning to Ψ, the most abundant nucleoside modification in mammalian RNA and relevant medically, we observed that RNase T2 processing of Ψ-containing RNA was strongly impaired. A similar result was seen with m^{1}Ψ. These findings were

Figure 6. Ψ inhibits the release of 2′,3′-cGMP for TLR7 activation

(A) pDCs were stimulated as indicated in the presence or absence of M5049. After 24 h, hIFNα2 release was detected. Data are depicted as mean ± SEM of $n = 3$ independent donors.

(B) CAL-1 cells of indicated genotypes were unstimulated or stimulated with OVA IVT-U, OVA IVT-Ψ, OVA IVT-m^{1}Ψ, and CpG^O. After 16 h, hIFN-β release was determined. Mean ± SEM of $n = 3$ independent experiments.

(C) Scheme of 2′,3′-cGMP release from ssRNA by RNase T2 and PLD exonucleases.

(D) IVT-U, IVT- Ψ, and IVT-m^{1}Ψ were digested with RNase T2 (0.5 nM), PLD3 (25 nM), or a combination of RNase T2 (0.5 nM) and PLD3 (25 nM) for 1 h and the release of 2′,3′-cGMP was analyzed by LC-MS. Mean ± SEM of $n = 3$ independent experiments.

(E) Scheme of the workflow for detecting single nucleotides in cells after transfection.

(F) 2′,3′-cGMP release in pDCs detected by LC-MS after transfection with OVA IVT-U or OVA IVT-Ψ. From each donor data were normalized to stimulation with OVA IVT-U and are depicted as mean ± SEM of $n = 3$ independent donors.

(G) CAL-1 cells of indicated genotypes were stimulated as indicated. After 16 h, TNF release was determined. Mean ± SEM of $n = 6$ independent experiments.

(H) RNA9.2s oligonucleotides from (G) were incubated in assay buffer or were digested with a combination of RNase T2 (10 nM) and PLD3 (25 nM) for 30 min and the release of 2′,3′-cGMP was analyzed by LC-MS. Mean ± SEM of $n = 3$ independent experiments.

(I) Scheme of ligand binding to TLR7 ectodomain.

(J) CAL-1 cells of indicated genotypes were unstimulated or stimulated with 2′,3′-cGMP (0.5 mM), short ORNs, or ORNs in combination with 2′,3′-cGMP (0.5 mM). Mean ± SEM of $n = 3$ independent experiments.

(K) Scheme of mouse injection followed by serum IFNα measurement.

(L) Pan-mIFNα release detected in the serum of Tlr13$^{-/-}$ mice injected with PBS, OVA IVT-U, or OVA IVT-m^{1}Ψ. Data are depicted as mean ± SEM of $n = 6$ (PBS), $n = 3$ (IVT-U), and $n = 6$ (IVT-m^{1}Ψ) Tlr13$^{-/-}$ mice. Statistical analysis was conducted by one-way ANOVA with Tukey's multiple comparison tests.

(M) Pan-mIFNα release detected in the serum of Tlr13$^{-/-}$ or Tlr13$^{-/-}$ × Rnaset2$^{-/-}$ mice injected with OVA IVT-U. Data are depicted as mean ± SEM of $n = 6$ (Tlr13$^{-/-}$) and $n = 4$ (*Tlr13*$^{-/-}$ × *Rnaset2*$^{-/-}$) mice. Statistical analysis was conducted by an unpaired t test.

See also Figures S5 and S6.

confirmed in long, complex RNA molecules, including those in the size range of mRNA vaccines. Reflecting its non-redundant role upstream of TLR7 and TLR8, the lack of cleavage of Ψ- and $m^1Ψ$-containing RNAs correlated with absent immunostimulatory activity. Indeed, introducing a single Ψ into an RNA oligonucleotide containing an RNase T2 motif substantially reduced both cleavage and the TLR7/8 response in cells. Tracking the fate of RNA in primary cells, we observed that Ψ-modified RNA no longer yielded the TLR7 agonist 2′,3′-cGMP. In this context, we also found that PLD exonucleases, which are essential upstream of TLR7 to release 2′,3′-cGMP from RNase T2-cleaved RNA, were similarly unable to degrade Ψ- and $m^1Ψ$-containing RNA, further contributing to the immune evasion of these modifications. Supporting these cellular observations, unmodified mRNA elicited a strong type I IFN response in mice, which was largely blunted in RNase T2-deficient animals.

Our results indicate that Ψ-modified RNA loses its stimulatory activity because it is not properly processed by RNase T2 and PLD exonucleases to generate TLR7 and TLR8 agonistic molecules. However, this does not rule out the possibility that Ψ-modified RNA may also fail to act as a ligand at the level of TLR7 and TLR8. To investigate this, we directly stimulated human monocytes with high concentrations of U, Ψ, or $m^1Ψ$ as potential agonists for the first binding pocket of TLR8. While these stimulatory conditions may not fully reflect the physiological engagement of TLR8 by incoming RNA and its degradation products, they provided an experimental setup to assess the activatability of TLR8 in a cellular context. Although U exhibited significantly lower potency compared with synthetic pocket 1 agonists, it still produced similar efficacies, making this an informative experiment. Using this setup, we found that Ψ was completely inactive in activating TLR8 compared with U, whereas, unexpectedly, $m^1Ψ$ displayed comparable activity. Interestingly, while Ψ alone failed to activate TLR8, it could enhance the TLR8-dependent RNA response, suggesting that Ψ may bind to TLR8 pocket 1 when released from ssRNA. A biochemical assay examining TLR8 dimerization in response to these nucleosides confirmed these findings: U and $m^1Ψ$ induced comparable TLR8 dimerization across a range of ligand concentrations, whereas Ψ alone exhibited little to no receptor dimerization activity. However, in combination with ssRNA, Ψ was still able to induce TLR8 dimerization *in vitro*. On the other hand, Ψ-containing RNA failed to activate TLR7 in PLD-deficient CAL-1 cells when stimulated with 2′,3′-cGMP, suggesting that Ψ-oligos do not bind to the second binding pocket of TLR7. Taken together, these findings suggest that Ψ-modified RNA is immune stealth for at least two reasons: first, its processing by RNase T2 and PLD exonucleases is significantly impaired, and second, Ψ itself is a weak agonist for the first binding pocket of TLR8, while Ψ-containing RNA does not serve as an agonist for the second binding pocket of TLR7. Interestingly, and somewhat unexpectedly, while the therapeutically relevant $m^1Ψ$ modification also resists RNase T2 and PLD exonuclease cleavage, it nonetheless functions as a TLR8 pocket 1 agonist.

In the absence of substrate-bound structures, it remains unclear how RNase T2 or PLD exonucleases distinguish U from Ψ. Ψ's N1 acts as an additional hydrogen bond donor, altering hydration and promoting intramolecular interactions with the RNA phosphate backbone. We and others[29] also observed Ψ-mediated base stacking with the 3′ neighboring nucleotide. These changes favor an A-form helical conformation, possibly explaining Ψ-RNA's poor substrate compatibility with PLD enzymes. For RNase T2, we further hypothesize that Ψ-induced conformational changes disrupt base coordination in the B2 pocket. Similar structural effects have been shown to inhibit RNase E cleavage,[34] where Ψ substitution adjacent to the cleavage site constrains the backbone and impairs catalytic site binding. A parallel mechanism may apply to PLDs and RNase T2, where Ψ-RNA adopts an unfavorable conformation for substrate binding. Interestingly, RNase A enzymes are unaffected by Ψ, suggesting that these structural alterations do not broadly impair lysosomal nuclease activity. Whether $m^1Ψ$ induces stacking or conformational changes like Ψ remains underexplored, though some evidence suggests similar effects.[35] The N1 methyl group in $m^1Ψ$ introduces steric bulk, potentially influencing its fit in RNase T2's B2 pocket. Notably, TLR8's responsiveness to $m^1Ψ$ but not Ψ is structurally unexpected. In the TLR8-U complex,[4] U adopts a syn conformation. This would position Ψ's N1 (or the methyl group of $m^1Ψ$) near Tyr353, which π stacks with the pyrimidine ring. Why this allows binding of $m^1Ψ$ but not Ψ remains unresolved, warranting further structural studies.

In conclusion, our study provides the first molecular insights into how Ψ evades immune recognition by RNA-sensing TLRs. We show that lysosomal nucleases fail to adequately process Ψ-containing RNA into TLR-agonistic ligands, highlighting their critical upstream role in non-self-RNA detection. Additionally, TLR8 bypasses Ψ in its first binding pocket, while TLR7 neglects Ψ-containing fragments in its second pocket, providing a secondary safeguard. Notably, $m^1Ψ$ also evades processing by these nucleases, yet retains the ability to activate TLR8. Taken together, these findings define the molecular basis for selective RNA recognition by TLRs and support the rational design of immunostealth mRNAs by avoiding RNase T2-dependent processing.

Limitations of the study

It is tempting to speculate that Ψ modification of endogenous RNA contributes to the non-responsiveness of TLR7 and TLR8 to self-RNA. Supporting this idea, pseudouridylation follows specific sequence motifs that may underlie self-non-self-discrimination. In eukaryotes, Ψ is introduced either by box H/ACA ribonucleoproteins or by sequence-specific Ψ synthases (PUS enzymes),[9] such as Pus1 targeting RU motifs[36] or Pus7 targeting UGUA motifs.[37] Although these patterns may aid self-recognition, their contribution is difficult to test due to the redundancy and essentiality of the pseudouridylation machinery. Indeed, additional modifications, like 2′-O-methylation, may also help render self-RNA non-immunogenic. Future studies will be needed to dissect the relative contributions of Ψ and other modifications to TLR7/8 evasion. Another important limitation to note is that, while our study reveals why Ψ-RNA fails to activate TLR7 and TLR8, it was not designed to assess RNase T2's role *in vivo* during responses to unmodified mRNA vaccines. Thus, we cannot infer its impact on adaptive responses, such as antibody or T cell induction. Nonetheless, elucidating RNase T2 function in this context may inform strategies to optimize mRNA vaccine efficacy.

RESOURCE AVAILABILITY

Lead contact

Further information and requests for resources and reagents should be directed to and will be fulfilled by the lead contact, Veit Hornung (hornung@genzentrum.lmu.de).

Materials availability

All newly generated materials associated with the paper are available upon request from the lead contact.

Data and code availability

This paper does not report any original code. Any additional information required to reanalyze the data reported in this work is available from the lead contact upon request.

ACKNOWLEDGMENTS

We thank Claudia Ludwig for technical support in isolating primary cells and Tobias Komar for his help in purifying TLR8 ECD (both Gene Center, LMU). This work was supported by grants from the Deutsche Forschungsgemeinschaft (DFG, German Research Foundation) CRC 237/A27 (project-ID 369799452) to V.H. and T.C., CRC 237/A05 (project-ID 369799452) to K.-P.H, CRC 1309/A02 (project-ID 325871075) to M.S., CRC 1309/A04 (project-ID 325871075) to T.C., and CRC 1361/P2 (project-ID 393547839) to T.C., grants from the ERC (ERC-2016-ADG-741912 EpiR) to T.C. and (ERC-2020-ADG–101018672 ENGINES) to V.H., and grants from the Federal Ministry of Education and Research (BMBF) in the framework of the Cluster4future program (CNATM – Cluster for Nucleic Acid Therapeutics Munich) (grant-ID 03ZU1201AA) to T.C., K.-P.H., and V.H.

AUTHOR CONTRIBUTIONS

Conceptualization, M.B., M.W., W.G., and V.H.; investigation, M.B., M.W., W.G., I.P., J.G., L.H., C.M.-H., M.H., A.P., A.J.T., G.W., and V.H.; writing, M.B. and V.H. with input from all authors; resources, K.-P.H., M.S., D.A., T.C., and V.H.; funding acquisition, V.H.; supervision, V.H.

DECLARATION OF INTERESTS

The authors declare no competing interests.

DECLARATION OF GENERATIVE AI AND AI-ASSISTED TECHNOLOGIES IN THE WRITING PROCESS

Portions of this manuscript were edited for clarity and conciseness using OpenAI's ChatGPT. The AI-assisted modifications were restricted to improving readability and conciseness, with all scientific content and conclusions remaining the sole responsibility of the authors.

STAR★METHODS

Detailed methods are provided in the online version of this paper and include the following:

Received: July 7, 2024
Revised: March 15, 2025
Accepted: May 22, 2025

REFERENCES

1. Fitzgerald, K.A., and Kagan, J.C. (2020). Toll-like Receptors and the Control of Immunity. Cell *180*, 1044–1066. https://doi.org/10.1016/j.cell.2020.02.041.
2. Heil, F., Hemmi, H., Hochrein, H., Ampenberger, F., Kirschning, C., Akira, S., Lipford, G., Wagner, H., and Bauer, S. (2004). Species-specific recognition of single-stranded RNA via toll-like receptor 7 and 8. Science *303*, 1526–1529. https://doi.org/10.1126/science.1093620.
3. Hemmi, H., Takeuchi, O., Kawai, T., Kaisho, T., Sato, S., Sanjo, H., Matsumoto, M., Hoshino, K., Wagner, H., Takeda, K., et al. (2000). A Toll-like receptor recognizes bacterial DNA. Nature *408*, 740–745. https://doi.org/10.1038/35047123.
4. Tanji, H., Ohto, U., Shibata, T., Taoka, M., Yamauchi, Y., Isobe, T., Miyake, K., and Shimizu, T. (2015). Toll-like receptor 8 senses degradation products of single-stranded RNA. Nat. Struct. Mol. Biol. *22*, 109–115. https://doi.org/10.1038/nsmb.2943.
5. Zhang, Z., Ohto, U., Shibata, T., Krayukhina, E., Taoka, M., Yamauchi, Y., Tanji, H., Isobe, T., Uchiyama, S., Miyake, K., et al. (2016). Structural Analysis Reveals that Toll-like Receptor 7 Is a Dual Receptor for Guanosine and Single-Stranded RNA. Immunity *45*, 737–748. https://doi.org/10.1016/j.immuni.2016.09.011.
6. Zhang, Z., Ohto, U., Shibata, T., Taoka, M., Yamauchi, Y., Sato, R., Shukla, N.M., David, S.A., Isobe, T., Miyake, K., et al. (2018). Structural Analyses of Toll-like Receptor 7 Reveal Detailed RNA Sequence Specificity and Recognition Mechanism of Agonistic Ligands. Cell Rep. *25*, 3371–3381. https://doi.org/10.1016/j.celrep.2018.11.081.
7. Greulich, W., Wagner, M., Gaidt, M.M., Stafford, C., Cheng, Y., Linder, A., Carell, T., and Hornung, V. (2019). TLR8 Is a Sensor of RNase T2 Degradation Products. Cell *179*, 1264–1275. https://doi.org/10.1016/j.cell.2019.11.001.
8. Bérouti, M., Lammens, K., Heiss, M., Hansbauer, L., Bauernfried, S., Stöckl, J., Pinci, F., Piseddu, I., Greulich, W., Wang, M., et al. (2024). Lysosomal endonuclease RNase T2 and PLD exonucleases cooperatively generate RNA ligands for TLR7 activation. Immunity *57*, 1482–1496. https://doi.org/10.1016/j.immuni.2024.04.010.
9. Borchardt, E.K., Martinez, N.M., and Gilbert, W.V. (2020). Regulation and Function of RNA Pseudouridylation in Human Cells. Annu. Rev. Genet. *54*, 309–336. https://doi.org/10.1146/annurev-genet-112618-043830.

10. Karikó, K., Buckstein, M., Ni, H., and Weissman, D. (2005). Suppression of RNA recognition by Toll-like receptors: the impact of nucleoside modification and the evolutionary origin of RNA. Immunity *23*, 165–175. https://doi.org/10.1016/j.immuni.2005.06.008.

11. Weissman, D., Ni, H., Scales, D., Dude, A., Capodici, J., McGibney, K., Abdool, A., Isaacs, S.N., Cannon, G., and Karikó, K. (2000). HIV gag mRNA transfection of dendritic cells (DC) delivers encoded antigen to MHC class I and II molecules, causes DC maturation, and induces a potent human in vitro primary immune response. J. Immunol. *165*, 4710–4717. https://doi.org/10.4049/jimmunol.165.8.4710.

12. Karikó, K., Muramatsu, H., Welsh, F.A., Ludwig, J., Kato, H., Akira, S., and Weissman, D. (2008). Incorporation of pseudouridine into mRNA yields superior nonimmunogenic vector with increased translational capacity and biological stability. Mol. Ther. *16*, 1833–1840. https://doi.org/10.1038/mt.2008.200.

13. Kormann, M.S., Hasenpusch, G., Aneja, M.K., Nica, G., Flemmer, A.W., Herber-Jonat, S., Huppmann, M., Mays, L.E., Illenyi, M., Schams, A., et al. (2011). Expression of therapeutic proteins after delivery of chemically modified mRNA in mice. Nat. Biotechnol. *29*, 154–157. https://doi.org/10.1038/nbt.1733.

14. Anderson, B.R., Muramatsu, H., Nallagatla, S.R., Bevilacqua, P.C., Sansing, L.H., Weissman, D., and Karikó, K. (2010). Incorporation of pseudouridine into mRNA enhances translation by diminishing PKR activation. Nucleic Acids Res. *38*, 5884–5892. https://doi.org/10.1093/nar/gkq347.

15. Anderson, B.R., Muramatsu, H., Jha, B.K., Silverman, R.H., Weissman, D., and Karikó, K. (2011). Nucleoside modifications in RNA limit activation of 2′-5′-oligoadenylate synthetase and increase resistance to cleavage by RNase L. Nucleic Acids Res. *39*, 9329–9338. https://doi.org/10.1093/nar/gkr586.

16. Andries, O., Mc Cafferty, S., De Smedt, S.C., Weiss, R., Sanders, N.N., and Kitada, T. (2015). N(1)-methylpseudouridine-incorporated mRNA outperforms pseudouridine-incorporated mRNA by providing enhanced protein expression and reduced immunogenicity in mammalian cell lines and mice. J. Control. Release *217*, 337–344. https://doi.org/10.1016/j.jconrel.2015.08.051.

17. Cappannini, A., Ray, A., Purta, E., Mukherjee, S., Boccaletto, P., Moafinejad, S.N., Lechner, A., Barchet, C., Klaholz, B.P., Stefaniak, F., et al. (2024). MODOMICS: a database of RNA modifications and related information. 2023 update. Nucleic Acids Res. *52*, D239–D244. https://doi.org/10.1093/nar/gkad1083.

18. Taoka, M., Nobe, Y., Yamaki, Y., Sato, K., Ishikawa, H., Izumikawa, K., Yamauchi, Y., Hirota, K., Nakayama, H., Takahashi, N., et al. (2018). Landscape of the complete RNA chemical modifications in the human 80S ribosome. Nucleic Acids Res. *46*, 9289–9298. https://doi.org/10.1093/nar/gky811.

19. Svitkin, Y.V., Cheng, Y.M., Chakraborty, T., Presnyak, V., John, M., and Sonenberg, N. (2017). N1-methyl-pseudouridine in mRNA enhances translation through eIF2alpha-dependent and independent mechanisms by increasing ribosome density. Nucleic Acids Res. *45*, 6023–6036. https://doi.org/10.1093/nar/gkx135.

20. Mauger, D.M., Cabral, B.J., Presnyak, V., Su, S.V., Reid, D.W., Goodman, B., Link, K., Khatwani, N., Reynders, J., Moore, M.J., et al. (2019). mRNA structure regulates protein expression through changes in functional half-life. Proc. Natl. Acad. Sci. USA *116*, 24075–24083. https://doi.org/10.1073/pnas.1908052116.

21. Fotin-Mleczek, M., Duchardt, K.M., Lorenz, C., Pfeiffer, R., Ojkić-Zrna, S., Probst, J., and Kallen, K.J. (2011). Messenger RNA-based vaccines with dual activity induce balanced TLR-7 dependent adaptive immune responses and provide antitumor activity. J. Immunother. *34*, 1–15. https://doi.org/10.1097/CJI.0b013e3181f7dbe8.

22. Kallen, K.J., Heidenreich, R., Schnee, M., Petsch, B., Schlake, T., Thess, A., Baumhof, P., Scheel, B., Koch, S.D., and Fotin-Mleczek, M. (2013). A novel, disruptive vaccination technology: self-adjuvanted RNActive((R)) vaccines. Hum. Vaccin. Immunother. *9*, 2263–2276. https://doi.org/10.4161/hv.25181.

23. Kranz, L.M., Diken, M., Haas, H., Kreiter, S., Loquai, C., Reuter, K.C., Meng, M., Fritz, D., Vascotto, F., Hefesha, H., et al. (2016). Systemic RNA delivery to dendritic cells exploits antiviral defence for cancer immunotherapy. Nature *534*, 396–401. https://doi.org/10.1038/nature18300.

24. Pollard, C., Rejman, J., De Haes, W., Verrier, B., Van Gulck, E., Naessens, T., De Smedt, S., Bogaert, P., Grooten, J., Vanham, G., et al. (2013). Type I IFN counteracts the induction of antigen-specific immune responses by lipid-based delivery of mRNA vaccines. Mol. Ther. *21*, 251–259. https://doi.org/10.1038/mt.2012.202.

25. Pepini, T., Pulichino, A.M., Carsillo, T., Carlson, A.L., Sari-Sarraf, F., Ramsauer, K., Debasitis, J.C., Maruggi, G., Otten, G.R., Geall, A.J., et al. (2017). Induction of an IFN-Mediated Antiviral Response by a Self-Amplifying RNA Vaccine: Implications for Vaccine Design. J. Immunol. *198*, 4012–4024. https://doi.org/10.4049/jimmunol.1601877.

26. Ostendorf, T., Zillinger, T., Andryka, K., Schlee-Guimaraes, T.M., Schmitz, S., Marx, S., Bayrak, K., Linke, R., Salgert, S., Wegner, J., et al. (2020). Immune Sensing of Synthetic, Bacterial, and Protozoan RNA by Toll-like Receptor 8 Requires Coordinated Processing by RNase T2 and RNase 2. Immunity *52*, 591–605.e6. https://doi.org/10.1016/j.immuni.2020.03.009.

27. Nunes, I.V., Breitenbach, L., Pawusch, S., Eigenbrod, T., Ananth, S., Schad, P., Fackler, O.T., Butter, F., Dalpke, A.H., and Chen, L.S. (2024). Bacterial RNA sensing by TLR8 requires RNase 6 processing and is inhibited by RNA 2′O-methylation. EMBO Rep. *25*, 4674–4692. https://doi.org/10.1038/s44319-024-00281-9.

28. Lu, H., Dietsch, G.N., Matthews, M.A.H., Yang, Y., Ghanekar, S., Inokuma, M., SUni, M., Maino, V.C., Henderson, K.E., Howbert, J.J., et al. (2012). VTX-2337 is a novel TLR8 agonist that activates NK cells and augments ADCC. Clin. Cancer Res. *18*, 499–509. https://doi.org/10.1158/1078-0432.CCR-11-1625.

29. Davis, D.R. (1995). Stabilization of RNA stacking by pseudouridine. Nucleic Acids Res. *23*, 5020–5026. https://doi.org/10.1093/nar/23.24.5020.

30. Chatterjee, S., Kon, E., Sharma, P., and Peer, D. (2024). Endosomal escape: A bottleneck for LNP-mediated therapeutics. Proc. Natl. Acad. Sci. USA *121*, e2307800120. https://doi.org/10.1073/pnas.2307800120.

31. Gomez-Diaz, C., Greulich, W., Wefers, B., Wang, M., Bolsega, S., Effern, M., Varga, D.P., Han, Z., Chen, M., Bérouti, M., et al. (2025). RNase T2 restricts TLR13-mediated autoinflammation in vivo. J. Exp. Med. *222*, e20241424. https://doi.org/10.1084/jem.20241424.

32. Sato, R., Liu, K., Shibata, T., Hoshino, K., Yamaguchi, K., Miyazaki, T., Hiranuma, R., Fukui, R., Motoi, Y., Fukuda-Ohta, Y., et al. (2025). RNase T2 deficiency promotes TLR13-dependent replenishment of tissue-protective Kupffer cells. J. Exp. Med. *222*, e20230647. https://doi.org/10.1084/jem.20230647.

33. Tong, A.J., Leylek, R., Herzner, A.M., Rigas, D., Wichner, S., Blanchette, C., Tahtinen, S., Kemball, C.C., Mellman, I., Haley, B., et al. (2024). Nucleotide modifications enable rational design of TLR7-selective ligands by blocking RNase cleavage. J. Exp. Med. *221*, e20230341. https://doi.org/10.1084/jem.20230341.

34. Islam, M.S., Bandyra, K.J., Chao, Y., Vogel, J., and Luisi, B.F. (2021). Impact of pseudouridylation, substrate fold, and degradosome organization on the endonuclease activity of RNase E. RNA *27*, 1339–1352. https://doi.org/10.1261/rna.078840.121.

35. Nivedita, D., Indrajit, D., Joanna, S., and Ansuman, L. (2023). Structural and thermodynamic consequences of base pairs containing pseudouridine and N1-methylpseudouridine in RNA duplexes. Preprint at bioRxiv. https://doi.org/10.1101/2023.03.19.533340.

36. Carlile, T.M., Martinez, N.M., Schaening, C., Su, A., Bell, T.A., Zinshteyn, B., and Gilbert, W.V. (2019). mRNA structure determines modification by pseudouridine synthase 1. Nat. Chem. Biol. *15*, 966–974. https://doi.org/10.1038/s41589-019-0353-z.

37. Carlile, T.M., Rojas-Duran, M.F., Zinshteyn, B., Shin, H., Bartoli, K.M., and Gilbert, W.V. (2014). Pseudouridine profiling reveals regulated mRNA pseudouridylation in yeast and human cells. Nature *515*, 143–146. https://doi.org/10.1038/nature13802.

38. Rapino, F., Robles, E.F., Richter-Larrea, J.A., Kallin, E.M., Martinez-Climent, J.A., and Graf, T. (2013). C/EBPalpha induces highly efficient macrophage transdifferentiation of B lymphoma and leukemia cell lines and impairs their tumorigenicity. Cell Rep. *3*, 1153–1163. https://doi.org/10.1016/j.celrep.2013.03.003.

39. Maeda, T., Murata, K., Fukushima, T., Sugahara, K., Tsuruda, K., Anami, M., Onimaru, Y., Tsukasaki, K., Tomonaga, M., Moriuchi, R., et al. (2005). A novel plasmacytoid dendritic cell line, CAL-1, established from a patient with blastic natural killer cell lymphoma. Int. J. Hematol. *81*, 148–154. https://doi.org/10.1532/ijh97.04116.

40. Schmid-Burgk, J.L., Schmidt, T., Gaidt, M.M., Pelka, K., Latz, E., Ebert, T.S., and Hornung, V. (2014). OutKnocker: a web tool for rapid and simple genotyping of designer nuclease edited cell lines. Genome Res. *24*, 1719–1723. https://doi.org/10.1101/gr.176701.114.

41. Baiersdörfer, M., Boros, G., Muramatsu, H., Mahiny, A., Vlatkovic, I., Sahin, U., and Karikó, K. (2019). A Facile Method for the Removal of dsRNA Contaminant from In Vitro-Transcribed mRNA. Mol. Ther. Nucleic Acids *15*, 26–35. https://doi.org/10.1016/j.omtn.2019.02.018.

42. Li, X.D., and Chen, Z.J. (2012). Sequence specific detection of bacterial 23S ribosomal RNA by TLR13. eLife *1*, e00102. https://doi.org/10.7554/eLife.00102.

Please cite this article in press as: Bérouti et al., Pseudouridine RNA avoids immune detection through impaired endolysosomal processing and TLR engagement, Cell (2025), https://doi.org/10.1016/j.cell.2025.05.032

CellPress
OPEN ACCESS

STAR★METHODS

KEY RESOURCES TABLE

REAGENT or RESOURCE	SOURCE	IDENTIFIER
Antibodies		
Anti dsRNA Antibody, clone rJ2	Sigma-Aldrich	Cat# MABE1134-25UL; RRID: AB_2819101
Anti mouse IgG, HRP linked antibody	Cell Signaling Technology	Cat# #7076; RRID: AB_330924
Chemicals, peptides, and recombinant proteins		
Acetonitrile	Carl Roth	Cat# HN40.1
Advanced RPMI 1640 medium	Gibco	Cat# 12633020
Ammonium persulfate	Sigma-Aldrich	Cat# A3678
BioColl	Bio&Sell	Cat# BS.L 6115
Blasticidin	Thermo Scientific	Cat# A1113903
CaptureSelect™ C-tagXL Affinity Matrix	Thermo Scientific	Cat# 2943072010
CD14 MircroBeads Human	Miltenyi	Cat# 130-050-201
Cellulose fibers	Merck	Cat#C6288-100G
Coomassie Brilliant Blue R-250 Dye	Thermo Scientific	Cat# 20278
CU-CPT9a	Invivogen	Cat# inh-cc9a
Express Five® SFM (1x)	Gibco	Cat# 10486025
Fetal calf serum	Gibco	Cat# 10270106
FuGene® Transfection Reagent	Promega	Cat# E2691
GlutaMAX	Gibco	Cat# 10270106
HEPES	Sigma-Aldrich	Cat# H0887-100ml
vivo-jetRNA®	VWR	Cat#76579-662
LPS-EB Ultrapure	InvivoGen	Cat#tlrl-3pelps
MEM NEAA	Gibco	Cat# 11140035
M5049	Invivogen	Cat# inh-m5049
N1-Methylpseudouridine	Sigma-Aldrich	Cat# SMB01360
N1-Methylpseudo UTP	Jena Bioscience	Cat#NU-890S
Opti-MEMTM	Gibco	Cat# 31985047
Penicillin/Streptomycin	Gibco	Cat# 15-140-122
Poly-L-arginine	Sigma-Aldrich	Cat#P7762
Pseudouridine	Sigma-Aldrich	Cat# SMB00912
Pseudo-UTP solution 100 mM	Jena Bioscience	Cat#NU-1139S
Recombinant Human IL-3	MPI of Biochemistry, Munich	N/A
Recombinant Human CSF1 (M-CSF)	MPI of Biochemistry, Munich	N/A
Recombinant Human RNase 1	MPI of Biochemistry, Munich	N/A
Recombinant Human RNase 2	MPI of Biochemistry, Munich	N/A
Recombinant Human RNase 6	MPI of Biochemistry, Munich	N/A
Recombinant Human TLR8 (AA27-827)	This study	N/A
RBC lysis Buffer	BioLegend	Cat# 420301
RPMI 1640 medium	Gibco	Cat# 11875093
R848	InvivoGen	Cat# tlrl-r848
SequaGel Concentrate	National diagnostics	Cat#EC830-1l
SequaGel Buffer	National diagnostics	Cat# EC835-200ml
SequaGel Diluent	National diagnostics	Cat# EC840-1l
Sf-900TM III SFM	Gibco	Cat# 12658019
Sodium pyruvate	Gibco	Cat# 11360039
SYBR Gold Nucleic Acid Gel Stain	Thermo Fisher Scientifc	Cat# S33102

(*Continued on next page*)

Please cite this article in press as: Bérouti et al., Pseudouridine RNA avoids immune detection through impaired endolysosomal processing and TLR engagement, Cell (2025), https://doi.org/10.1016/j.cell.2025.05.032

Continued

REAGENT or RESOURCE	SOURCE	IDENTIFIER
TEMED	Carl Roth	Cat# 2367.3
TL8-506	InvivoGen	Cat# tlrl-tl8506
TRIS glycine SDS-PAGE	Thermo Scientific	Cat# XP00125BOX
Uridine	Sigma-Aldrich	Cat# U3750
β-Estradiol	Sigma-Aldrich	Cat#E8875
2x RNA loading dye	Thermo Fisher Scientific	Cat# R0641
5-Propargylamino-CTP-PEG5-AZDye488	Jena Bioscience	Cat# NU-831-PEG5-AZ488
6x DNA loading dye	Thermo Fisher Scienctific	Cat#R1161
2′,3′-cGMP	BIOLOG	Cat# G 025-250
Critical commercial assays		
Ampliscribe-T7-flash-transcription kit	Lucigen	Cat# ASF3507
Faustovirus Capping Enzyme	New England Biolabs	Cat# M2081I
E. coli Poly(A) Polymerase	New England Biolabs	Cat# M0276I
Human IFN-β ELISA Set	R&D System	Cat# DY814-05
Human IFN-α2 ELISA Set	R&D System	Cat# DY9345-05
Human IL-6 ELISA Set	BD Biosciences	Cat# 555220
Human TNF ELISA Set	BD Biosciences	Cat# 555212
Human IP10 ELISA Set	BD Biosciences	Cat# 550926
BCA protein assay Kit	Thermo Fisher Scientific	Cat# 23227
Mouse IFN-alpha ELISA Kit	R&D Systems	Cat# 42120-1
CD34 MicroBead Kit UltraPure, human	Miltenyi	Cat# 130-100-453
Monarch RNA Cleanup Kit	New England Biolabs	Cat# T2050I
Experimental models: Cell lines		
BLaER1 human B-cell to monocyte trans-differentiation cell line	Rapino et al[3,8]	N/A
CAL-1	Maeda et al.[39]	N/A
SF21	Thermo Fisher Scientific	Cat#12682019
High Five™ Cells in Express Five™ Medium	Thermo Scientific	Cat# B85502
Oligonucleotides		
RNA40^{S}(rG*rC*rC*rC*rG*rU*rC*rU*rG* rU*rU*rG*rU*rG*rU*rG*rA*rC*rU*rC)	Miltenyi	130-104-429
RNA40^{O}(rGrCrCrCrGrUrCrUrGr UrUrGrUrGrUrGrArCrUrC)	IDT	N/A
RNA40i(rArCrCrCrArUrCrUrArUrUr ArUrArUrArGrCrUrC)	IDT	N/A
RNA9.2s(rArGrCrUrUrArArCrCrUrGr UrCrCrUrUrCrArA)	IDT	N/A
rArGrCrUrUrArArCrCrUrGrm UrCrCrUrUrCrArA	IDT	N/A
rArGrCrUrUrArArCrCrUrGrΨrCr CrUrUrCrArA	This study	N/A
rArGrCrΨrΨrArArCrCrΨrGrΨr CrCrUrUrCrArA	This study	N/A
rCrCrUrUrCrA(dAdC)$_7$	This study	N/A
rCrCrΨrΨrCrA(dAdC)$_7$	This study	N/A
(dAdC)$_7$rUrUrGrUrCrU	Ella Biotech	N/A
(dAdC)$_7$rUrUrGrmUrCrU	Ella Biotech	N/A
(dAdC)$_7$rUrUrGrUrmCrU	Ella Biotech	N/A
(dAdC)$_7$rUrUrGrΨrCrU	Ella Biotech	N/A

(*Continued on next page*)

Please cite this article in press as: Bérouti et al., Pseudouridine RNA avoids immune detection through impaired endolysosomal processing and TLR engagement, Cell (2025), https://doi.org/10.1016/j.cell.2025.05.032

CellPress
OPEN ACCESS

Continued

REAGENT or RESOURCE	SOURCE	IDENTIFIER
$(dAdC)_7$rUrUrGrm$^1\Psi$rCrU	Ella Biotech	N/A
rΨrΨrΨrArGrC	This study	N/A
rUrUrUrArGrC	This study	N/A
rUrUrUrArGrCrUrUrArAr CrCrUrGrUrCrCrUrU	IDT	N/A
rΨrΨrΨrArGrCrUrUrAr ArCrCrUrGrUrCrCrUrU	This study	N/A
m$^1\Psi$m$^1\Psi$m$^1\Psi$rArGrCrUr UrArArCrCrUrGrUrCrCrUrU	This study	N/A
$(dAdC)_7$rGrArGrUrArGrA	IDT	N/A
$(dAdC)_7$rGrArGrΨrArGrA	This study	N/A
rUrUrUrArGrCrUrUrAr ArCrCrUrGrUrCrCrUrU-FAM	Biomers	N/A
rΨrΨrΨrArGrCrUrUrArArCrCrUrGrUrCrCrUrU-FAM	Biomers	N/A
CpG O (TCGTCGTTTTGTCGTTTTGTCGTT	IDT	N/A
Recombinant DNA		
pACEBac1_IgK_hsTLR8(AA27-827)_EPEA	This study	N/A
Software and algorithms		
GraphPad Prism10	GraphPad	N/A
Outknocker	Schmid-Burgk et al.[40]	N/A
AcquireMP	Refeyn	N/A
FlowJo	BD Biosciences	N/A
Other		
Ultrafiltration spin columns, 0.45 μm cutoff	Merck	Cat# 20-218

METHOD DETAILS

Cell culture

BLaER1, THP-1, primary PBMCs, CD14$^+$ and pDCs were cultured in RPMI 1640 medium supplemented with 10% heat-inactivated fetal calf serum (FCS), 100 U/ml penicillin/streptomycin (PS), and 1 mM sodium pyruvate. CAL-1 cells were cultured in RPMI 1640 medium supplemented with 10% heat-inactivated fetal calf serum, 100 U/ ml penicillin/streptomycin (PS), 1 mM sodium pyruvate, 2x GlutaMAX, 10 mM HEPES and 1x MEM NEAA. The cells were maintained in a 37°C humidified incubator with a 5% CO_2 atmosphere. To induce the transformation of BLaER1 monocytes into macrophages, a cytokine cocktail - M-CSF (10 ng/ml), IL-3 (10 ng/ml) and 100 nM β-estradiol - was added to the culture for a period of 5 days. THP-1 cells were differentiated with PMA (100 ng/ml) for 16 h and rested for 2 days prior to stimulation. The differentiation process for both cell lines was carried out in a 96-well plate, with each well containing 80,000 cells. Afterwards, cells were used for various stimulation experiments.

SF21 insect cells were cultured in Sf-900™ III SFM (1x) medium supplemented with 100 U/ml penicillin/streptomycin (PS) and High5 insect cells were cultured in Express Five SFM (1x) medium supplemented with L-Glutamine (18 mM) and 100 U/ml penicillin/streptomycin (PS). Both cell lines were maintained in a shaking incubator (95 rpm) without CO_2.

Isolation of PBMCs, primary human monocytes and primary human pDCs

As previously described, peripheral blood mononuclear cells (PBMCs) were isolated from the leukocyte reduction system chambers left over from platelet donation from healthy donors. Approval from the relevant ethics committee and informed consent from all donors according to the Declaration of Helsinki were obtained (project number: 19-238, Ethics Committee of the Medical Faculty of Ludwig-Maximilians-University Munich). PBMCs were isolated using BioColl and erythrocyte lysis (RBC lysis buffer). Human monocytes purified by MACS from PBMCs using CD14 microbeads and human primary pDCs were MACS purified from PBMCs using CD304 microbeads.

Cell stimulation

CAL-1 cells (100,000 cells/well) and THP-1 cells were primed with IFN-γ (10 ng/ml) for 6 hours prior to stimulation. BLaER1 cells were stimulated after trans-differentiation and primary human PBMCs (400,000 cells/well), CD14$^+$ monocytes (100,000 cells/well) and pDCs (20,000 cells/well) were rested for 4 hours after isolation prior to stimulation. Primary pDCs were additionally treated with

IL-3 (10 ng/ml). For transfection with RNA40^{S} (0.6 μg/well), RNA40^{O} (1.2 μg/well), RNA9.2s and modified version of RNA9.2s (1.2 μg/well), short ORNs ((dAdC)$_7$UUGUCU, (dAdC)$_7$UUGmUCU, (dAdC)$_7$UUGUmCU, (dAdC)$_7$UUGΨCU, (dAdC)$_7$UUGm^{1}ΨCU, CCUUCA(dAdC)$_7$ and CCΨΨCA(dAdC)$_7$) (2.4 μg/well) and indicated Cas9 IVT (each 1.2 μg/well) or OVA IVT (each 0.6 μg/well) constructs, RNA and poly-L-arginine were incubated separately in a 1:1 ratio for 5 minutes in pre-warmed Opti-MEM (25 μl/well). After combining, the two reagents were incubated for additional 20 minutes before being added to the cells. To stimulate primary pDCs with OVA-IVT constructs using Lipofectamine instead of poly-L-arginine as transfection reagent, Lipofectamine2000 (0.5 μl/well) and OVA-IVTs (each 0.6 μg/well) were mixed and incubated in pre-warmed Opti-MEM (50 μl/well) for 20 min and afterwards added to the cells. For RNA transfections in the presence of the TLR specific inhibitors, CU-CPTa (final concentration: 10 μM) or M5049 (final concentration: 1 μM) was added to the cells 30 min prior to stimulation. Furthermore, cells were stimulated with 200 ng/ml LPS-EB ultrapure (Lipopolysaccharide from Escherichia coli 0111:B4), 0.5 mM 2′,3′-cGMP, 5 μM CpG^{O} and indicated concentrations of uridine, pseudourdine (Ψ), N1-methylpseudouridine (m^{1}Ψ) and 2′-O-methyluridine (Um). To calculate EC$_{50}$ values (Figure 5B), BLaER1 monocytes were stimulated with the different nucleosides at concentrations ranging from 64 mM to 4 mM. Supernatants of CD14$^+$ monocytes were harvested after 24 hours of stimulation at 37 °C, the supernatants of BLaER1 cells were harvested after 14 hours and the supernatants of CAL-1 cells were harvested after 16 hours.

Baculovirus production

A codon optimized version of the Igκ leader sequence fused to the ectodomain of human TLR8 encompassing AA27-827 was obtained from Max Planck Institute (Munich) and cloned into pACEBac1 vector for bacmid preparation. Production of TLR8 baculovirus was conducted in SF21 insect cells. For transfection, 200 μl SF21 medium, 3 μl FuGene® and 2 μg of bacmid were combined and incubated for 45 min at room temperature. Next, the transfection mix was added dropwise to SF21 cells (0.4x10^6 cells/2 ml) and incubated at 27 °C. After three days, the supernatant (P0) was harvested, added to a cell suspension of SF21 cells (1x10^6 cells/ml, 10 ml in total) and shaken for three days at 27 °C at 95 rpm. Subsequently, the virus containing supernatant (P1) was collected and filtered. Next, P1 virus (0.5 ml) was added to 50 ml of SF21 suspension cells (0.4x10^6 cells/ml), which were shaken (95 rpm) for 3 days at 27 °C. The supernatant (P2) was collected, filtered and stored at 4°C.

Protein expression and purification

Expression of recombinant TLR8 ectodomain was induced for three days by adding P2 baculovirus (Dilution of virus: 1:200) to High5 cells (1x10^6 cells/m). Subsequently, the supernatant containing secreted TLR8 ectodomain was harvested and filtered. EPEA agarose beads were added to the supernatant and rotated for 2 hours at 4°C. The beads were washed three times with wash buffer (20 mM Tris pH=7.5, 150 mM NaCl) and the protein was eluted (20 mM Tris pH=7.5, 150 mM NaCl, 2M $MgCl_2$). Eluted TLR8 was dialyzed overnight (50 mM $NaHPO_4$, 100 mM NaCl pH=5.0) and concentrated to 10 μM. TLR8 was stored at 4°C prior to mass photometry measurements.

Coomassie staining of hsTLR8 (AA27-827)

To assess the purity of recombinant hsTLR8 (AA27-827), the protein was separated on a 12% TRIS glycine SDS-PAGE. The gel was subsequently stained with Coomassie (45% Ethanol, 10% acetic acid and 1g/L Coomassie Brilliant Blue R-250 Dye in milliQ water) for 1 hour at room temperature and destained again (20% Ethanol, 10% acetic acid in milliQ water) overnight.

Mass photometry

Mass photometric assays for hsTLR8 (AA27-827) ectodomain dimerization were performed using a Refeyn TwoMP mass photometer. Prior to each measurement, hsTLR8 (AA27-827) (10 μM) was incubated with indicated concentrations of uridine, pseudouridine, N1-methylpseudouridine or 2′-O-methyluridine or in combination with ssRNA40 (30 μM) for 10 min at room temperature. Prior to each measurement, the different samples were diluted to a final concentration of 50 nM hsTLR8 (AA27-827) in sterile filtered mass photometry buffer (50 mM $NaHPO_4$, 100 mM NaCl, pH=5.0). The measurements were recorded as 60-second movies and the resulting data were processed using AcquireMP software. All incubations and measurements were performed in triplicates, except for the incubation of single nucleosides in combination with ssRNA40 (Figure 5F, lower panel), which was performed in duplicates.

RNase assays

Unless otherwise stated, 100 ng of RNA was treated with indicated amounts of enzyme in assay buffer (50 mM NaAc, 100 mM NaCl, pH=4.5) or in IDTE buffer (10 mM Tris, 0.1 mM EDTA, pH=8) for 20 minutes at 37°C. Subsequently, 2x RNA loading dye was added to the mixture, which was then heated at 95°C for 5 additional minutes. The resulting fragments were separated and detected on a urea gel. For agarose gels, 1 μg of different Cas9 IVT constructs were incubated with indicated amounts of RNase T2 for 20 min at 37 °C. Afterwards 6x DNA loading dye was added, and 0.5 μg of RNA was loaded onto the agarose gel.

ELISA

hIL-6, hTNF, hIP-10, hIFNα2, hIFNβ and mIFNα ELISAs were conducted according to supplier's protocol. For TLR7 and TLR8 stimulation assays, we primarily used IFNα or IFNβ as readouts for TLR7 activation in plasmacytoid cell models and IL-6 for TLR8 activation in myeloid cells. These cytokines were selected as proximal indicators of pathway activation and have been shown to be robust readouts based on extensive prior experience.

Urea and agarose gels

Urea gels were prepared according to the manufacturer's instructions using SequaGel Concentrate, SequaGel Diluent, and SequaGel buffer. The gels were first run at 150 V for 10 minutes, followed by a 60-minute run at 250 V in 1x TBE buffer (containing 100 mM Tris, 100 mM boric acid, and 2 mM EDTA). The gels were then stained with SYBR Gold Nucleic Acid Gel Stain for 5 minutes, followed by imaging. 1% agarose gels were run for 40 min at 120 V prior to imaging.

Affinity measurement by fluorescence anisotropy

The Fluorescence anisotropy assay was carried out in a black 384-well flat-bottom plate with a total reaction volume of 50 μl. 3′-FAM-labeled substrates (10 nM) were incubated for 20 minutes at room temperature with increasing concentrations of PLD3(H201N, H416N) in assay buffer (50 mM sodium acetate, 100 mM NaCl, pH 4.5). After incubation, the change in anisotropy was measured at an excitation wavelength of 490 nm and an emission wavelength of 520 nm using an automated polarization microscope. Data was analyzed by fitting to a one site-specific binding model.

In vitro transcription

In vitro transcription of a ~2,500 bp Cas9 amplicon (forward primer: GACAAGAAGTACAGCAT-CGGCCTGG; reverse primer: CCACCCGAAATTAATACGACTCACTATAGGGAGACCAC-AACTGCAGGTAGTACAGGTACAGCTTC) was conducted according to supplier's protocol (Lucigen, #ASF3507), followed by DNase I treatment to remove the DNA template from the IVT. For IVT Ψ, IVT $m^1\Psi$, Pseudo-UTP and N^1-Methylpseudo-UTP was added to the reaction mix instead of UTP. For the fluorescently labeled IVT, the reaction mix contained 2.5 mM ATP, GTP, and UTP, along with 0.2 mM CTP and 0.1 mM 5-Propargylamino-CTP-PEG5-AZDye488. The fluorescently labeled RNA was purified using the Monarch RNA Cleanup Kit after DNase I treatment.

Sodium acetate precipitation of Cas9 IVT constructs

After IVT, glycogen (final concentration: 0.5 mg/ml), 3 M sodium acetate (1:10 volume) and 100% ethanol (4 volumes) were added to the nucleic acid solution. The reaction was mixed thoroughly after each addition of the three components and incubated for 16 hours at –20 °C. The precipitated RNA was centrifuged for 30 min at 4000 rpm at 4 °C. Subsequently, the supernatant was carefully discarded, and the pellet was washed twice by adding 500 μl of 80% cold ethanol. Lastly, the pellet was air dried and resuspended in water to a final concentration of 1 μg/μl. Prior to use it was confirmed that the RNA is fully intact by an agarose gel.

Purification of IVT mRNA using cellulose

To remove dsRNA contaminants from OVA-IVT RNAs, OVA-IVTs were purified by cellulose chromatography as previously described.[41] In brief, cellulose fibers were initially resuspended in RNase-free chromatography buffer (10 mM HEPES, pH 7.2, 0.1 mM EDTA, 125 mM NaCl, and 16% (v/v) ethanol) to a final concentration of 0.2 g/ml. Next, 700 μl of cellulose slurry was transferred to an ultrafiltration spin-column (0.45 μm cutoff) and centrifuged for 1 min at 14,000 x g. The flowthrough was discarded, the cellulose washed with 500 μl of chromatography buffer and centrifuged again for 1 min at 14,000 x g. Next, 200 μg of OVA-IVT RNA in 500 μl chromatography buffer was added to the washed cellulose into the spin column. The column was rotated on a spinning wheel for 30 min at room temperature and afterwards centrifuged for 1 min at 14,000 x g. The flowthrough, containing the purified RNA, was collected, and subjected to two more rounds of cellulose purification.

Finally, the RNA was precipitated by adding 50 μl of 3 M NaOAc (pH 5.5) and 500 μl of isopropanol and subsequent centrifugation at 16,000 x g for 2 hours at 4 °C. The recovered purified RNA was resuspended in nuclease free water. The removal of dsRNA contaminations was confirmed by RNA dot blot using an anti-dsRNA antibody.

Capping and Tailing of IVT mRNA

An m^7G cap (Cap-0) structure was added to the purified OVA IVT RNAs using the Faustovirus capping enzyme, following the supplier's protocol (NEB #M2081). Subsequently, IVTs were poly(A)-tailed using E. coli Poly(A) Polymerase, also following the supplier's protocol (NEB# M0276). RNA was purified after each step using the Monarch RNA Cleanup Kit.

Cellular RNA uptake assay

To determine the uptake of RNA upon transfection, GFP-negative BLaER1 monocyte-derived macrophages (80,000 cells/well) were stimulated with AZDye488-labeled RNAs (1.2 μg/well) using poly-L-arginine as a transfection reagent as described above. At 2 h post transfection, cells were detached and resuspended in FACS buffer (PBS+2% FCS). Subsequently, AZDye488-positive cells were analyzed using a BD FACS Melody™ flow cytometer. Data was analyzed using FlowJo software (BD Biosciences).

Mouse lines

Mice in this study were housed under specific pathogen-free (SPF) conditions at 21 ± 1°C, with a 12-hour light/dark cycle and an average humidity of 55%. Breeding and maintenance followed the regulations of the animal welfare authorities of the government of Upper Bavaria (application number: 55.2-2532.Vet_02-21-97). The mouse lines used were previously established, including $Tlr13^{-/-}$[42] and $Rnaset2^{-/-}$.[31] Experimental mice were between 40 and 80 weeks old.

Please cite this article in press as: Bérouti et al., Pseudouridine RNA avoids immune detection through impaired endolysosomal processing and TLR engagement, Cell (2025), https://doi.org/10.1016/j.cell.2025.05.032

In vivo injection of mRNA

OVA-mRNA for in vivo injections was complexed using in vivo-jet PEI® according to the manufacturer's protocol. Mice were then intravenously injected with 10 μg of mRNA per mouse. As a negative control, PBS was injected. $Tlr13^{-/-}$ mice that received PBS injections (Figure 6L) were later injected with U-IVT following a 7-day washout period. Six hours post-injection, blood was collected and left at room temperature for 45 to 60 minutes to allow natural clotting. The samples were then centrifuged at 1,000 × g for 10 minutes, and the serum was transferred to a clean tube for PAN-IFNα analysis via ELISA. All animal experiments were approved by the local regulatory agency (Regierung von Oberbayern, #55.2-2532-02-20-109).

RNase assays for LC-MS

RNA (1 μg) was digested with indicated concentrations of RNase T2 or RNase 1 for 20 min at 37°C in IDTE buffer (10 mM Tris, 0.1 mM EDTA, pH=8.0).

RNA isolation

All RNA isolation steps were performed at room temperature. Enzyme reactions (vol. of reaction mixture < 350 μl) were quenched by addition of 350 μl *Roti-Phenol* (phenol / chloroform / isoamyl alcohol; 25/24/1; *Roth*). milliQ water was added until a total sample volume of 700 μl was reached (aqueous phase / *Roti-Phenol*; 1/1; v/v). After vigorous vortexing (2 min) and centrifugation (10,000 x g; 1 min), the upper, aqueous phase was transferred to a new tube. 350 μl of milliQ water were added to the phenol/chloroform phase, again followed by vortexing (2 min) and centrifugation (10,000 x g; 1 min). The aqueous phases were combined, and 700 μl of chloroform were added (H_2O / chloroform; 1/1; v/v). The samples were vortexed (2 min), centrifuged (10,000 x g; 1 min), and the upper, aqueous layer was transferred to a new tube. This chloroform extraction step was repeated two more times. The resulting, clean aqueous phase was lyophilized overnight (*Alpha 2-4 LSCbasic, Christ*). The remaining residue was re-dissolved in 200 μl of milliQ water and again lyophilized overnight. Samples were then re-dissolved in 100 μl of milliQ water and stored at -78 °C until submission to LC-MS analysis (see below).

Liquid chromatography – mass spectrometry (LC-MS): general procedure

All samples were filtrated before measurement using an AcroPrep Advance 96 filter plate 0.2 μm Supor from Pall Life Sciences and were kept on ice during handling. HPLC-HESI-MS analyses were performed on a Dionex Ultimate 3000 HPLC system coupled to a Thermo Fisher LTQ Orbitrap XL mass spectrometer. Compounds of interest (injection volume: 85 μl) were separated with an Interchim Uptisphere120-3HDO C18 column whose temperature was maintained at 30 °C. Elution buffers were buffer X (2 mM NH_4HCOO in H_2O; pH 5.5) and buffer Y (2 mM NH_4HCOO in H_2O/MeCN 20/80 v/v; pH 5.5). Different and optimized HPLC gradients and flow rates were used for experiments involving 20mer RNA digests, 2,500 bp RNA digests, or chimeric DNA-RNA species (see below). Chromatograms were recorded at 260 nm with a Dionex Ultimate 3000 Diode Array Detector with a data collection rate of 20 Hz and a response time 0.10 s. The chromatographic eluent was directly injected into the ion source of the mass spectrometer without prior splitting. Ions were scanned in the positive polarity mode over a full-scan range of m/z = 225-2000 with a resolution of 100,000. Parameters of the mass spectrometer were tuned with a freshly mixed solution of inosine (5 μM) in buffer X. Source-dependent parameters were set as follows: Capillary temperature 275 °C; APCI vaporizer temperature 100 °C; sheath gas flow 5.00; auxiliary gas flow 21.0; sweep gas flow 1.00; source voltage 4.80 kV; capillary voltage 0 V; tube lens voltage 45.00 V. Data analysis was performed using the program Xcalibur from Thermo Scientific: Ion chromatograms of the compounds of interest were extracted from the total ion current (TIC) chromatogram with a mass range set to +/- 0.0100 u (Δm<3ppm) around m/z = [M+nH]/n (z =n; corresponding to the fragment $[M+nH]^{n+}$) of the compound's most abundant isotopologue (the isotopologue distribution of a compound was calculated with ChemDraw).

LC-MS analysis of RNA40/RNA40i/RNA9.2s and their cleavage products

This section outlines the LC-MS analysis methods used to generate the data shown in Figure 1. In this case, the HPLC gradient was as follows: 0→3 min, 0 % Y, 150 μl/min; 3→4 min, 0→0.1 % Y, 150 μl/min; 4→8 min, 0.1 % Y, 150 μl/min; 8→63 min, 0.1→6 % Y, 150 μl/min; 63→73 min, 6→15 % Y, 150 μl/min; 73→80 min, 15→75 % Y, 150→200 μl/min; 80→88 min, 75 % Y, 200 μl/min.

Two obstacles had to be overcome to identify and quantify the fragments: First, all isomers of a given base composition have the same mass. Second, although an optimized HPLC gradient was used, some fragments have similar retention times, so their UV absorption peaks overlap. Nevertheless, to identify and quantify all fragments, we first identified fragments with unique nucleotide composition (and mass) and with non-overlapping UV absorption peaks. Each of these fragments was quantified by integrating its UV absorption peak and dividing this value by its extinction coefficient (the extinction coefficients themselves were calculated using IDT's OligoAnalyzer). The value thus obtained is directly proportional to the absolute amount of the fragment in the sample. In addition, the total base compositions (but not the sequence) of all other fragments present were identified via their mass, and non-overlapping UV absorption peaks were integrated. The identity/sequence and the absolute amounts of all fragments present were then determined by applying the following logical principles: For any given cleavage site, the total amount of fragments with a 3′-end at this position must equal the total amount of fragments possessing the matching 5′-end. Furthermore, for each of the 20 nucleotide positions of the reactant strand, the total amount of all fragments containing a given nucleotide must add up to the same value (this value is the total amount/fraction of educt oligomer processed by RNase T2 or RNase 1, respectively). The same value should be obtained

at any cleavage site when adding up the amounts of fragments bearing a 3′-end (or a 5′-end, respectively) at this position and the amounts of all fragments not being cleaved at this site but instead containing both nucleotides of the cleavage site. Following these rules, all fragments present in the samples could unequivocally be identified, and their absolute amounts could be determined. The cleavage percentage at a given site was then calculated by dividing the total amount of fragments with a 3′-end at this position (or a 5′-end, respectively) by the total amount of educt oligomer processed by RNase T2 or RNase 1, respectively (i.e. sum of all 3′ fragments ending at a particular cleavage site divided by the sum of these 3′ fragments and of the fragments covering this cleavage site).

LC-MS analysis of a 2,500 nt RNA digested either by RNase T2 or RNase 1

This section outlines the LC-MS analysis methods used to generate the data shown in Figure 2. In this case, the HPLC gradient was as follows: 0→3 min, 0 % Y, 150→100 μl/min; 3→4 min, 0→0.1 % Y, 100 μl/min; 4→8 min, 0.1 % Y, 100 μl/min; 8→63 min, 0.1→6 % Y, 100 μl/min; 63→73 min, 6→15 % Y, 100 μl/min; 73→80 min, 15→75 % Y, 100→150 μl/min; 80→88 min, 75 % Y, 150→200 μl/min.

In these experiments, a plethora of cleavage products with similar retention times were generated. Since their UV-peaks were overlapping in most cases, an UV-based absolute quantification of fragments was not possible. We therefore decided to go for relative quantification. For di- and trimer identification, we designed 9 different RNA 5mers (UGUUU; UAUUU; UUGUU; GUCCC; AUCCC; UCGUU; UCAUU; UAGUU; UGAUU) and subjected them to digestion either by RNase T2 or RNase 1. The resulting cleavage products were dimers and trimers of a defined sequence (and mass). These were analyzed by LC-MS using the same HPLC gradient as for the 2,500 bp RNA analysis. This way, we obtained a data set correlating particular 2/3mer sequences (and masses) with their HPLC retention time. Based on this data set, the ratios of 16 dimers and 12 trimers in the samples (RNase T2 vs. RNase 1) were determined. Incidentally, in most cases, fragments of interest were either only present in the RNase T2 digest sample or in the RNase 1 digest sample. The resulting fragment ratio of 1:0 is the same as it would be based on absolute fragment amounts.

LC-MS analysis of chimeric DNA/RNA probes and their cleavage products

This section outlines the LC-MS analysis methods used to generate the data shown in Figure 3. In this case, the HPLC gradient was as follows: 0→3 min, 0 % Y, 150 μl/min; 3→4 min, 0→0.1 % Y, 150 μl/min; 4→8 min, 0.1 % Y, 150 μl/min; 8→53 min, 0.1→5 % Y, 150 μl/min; 53→70 min, 5→15 % Y, 150 μl/min; 70→73 min, 15→100 % Y, 150→200 μl/min; 73→77 min, 100 % Y, 200 μl/min. Identity /sequence of fragments and their absolute amounts were determined as in the case of the RNA40/RNA40i/RNA9.2s samples (see above). Here, and in contrast to the calculations done for RNA40/RNA40i/RNA9.2s, cleavage percentages were calculated considering the amount of non-processed chimeric educt oligomer, too: The cleavage percentage at a given site was calculated by dividing the total amount of fragments with a 3′-end at this position (or a 5′-end, respectively) by the sum of the total amount of educt oligomer processed by RNase T2 (or RNase 1, respectively) AND the amount of remaining/non-cleaved educt oligomer (otherwise, when calculated as for RNA40/RNA40i/RNA9.2s, a minimal cleaving at a single position would lead to a calculated cutting percentage of 100 %).

LC-MS/QQQ analysis of nucleoside-monophosphates)

This section outlines the LC-MS analysis methods used to generate the data shown in Figures 6D, 6F, and 6H. The preparation for LC-MS analysis to measure 2′,3′-cGMP *in vitro* released by PLD3 and RNase T2 and the subsequent analysis of the nucleoside-monophosphate by LC-MS/QQQ was conducted as previously described.[8]

Synthesis and purification of oligonucleotides

Phosphoramidites of canonical ribonucleosides (Bz-A-CE, Dmf-G-CE, Ac-C-CE and U-CE) were purchased from LinkTech and Sigma-Aldrich. Phosphoramidites of Ψ and $m^1Ψ$ were synthesized respectively. Oligonucleotides were synthesized on a 1 μmol scale using High Load Glen UnySupport™ as solid supports for strands employing an RNA automated synthesizer (Applied Biosystems 394 DNA/RNA Synthesizer) utilizing standard phosphoramidite chemistry. ONs were synthesized in DMT-OFF mode using DCA as a deblocking agent in CH_2Cl_2, BTT or Activator 42® as activator in MeCN, Ac_2O as capping reagent in pyridine/THF and I_2 as oxidizer in pyridine/H_2O.

The solid support beads were suspended in a 1:1 aqueous solution mixture (0.6 ml) of 30% NH_4OH and 40% $MeNH_2$. The suspension was heated at 65 °C for 60 min for High Load Glen UnySupport™. Subsequently, the supernatant was collected, and the beads were washed with water (2×0.3 ml). The combined aqueous solutions were concentrated under reduced pressure using a SpeedVac concentrator. The crude was dissolved in DMSO (100 μl) and triethylamine trihydrofluoride (125 μl) was added. The solution was heated at 65 °C for 1.5 h. Finally, the ON was precipitated by adding 3 M NaOAc in water (25 μl) and n-butanol (1 ml). The mixture was kept at -80 °C for 2 h and centrifuged at 4°C for 1 h. The supernatant was removed, and the white precipitate was lyophilized.

The crude was purified by semi-preparative HPLC (1260 Infinity II Manual Preparative LC System from Agilent equipped with a G7114A detector) using a reverse-phase (RP) VP 250/10 Nucleodur 100-5 C18ec column from Macherey-Nagel. Buffers: A) 0.1 M AcOH/Et_3N in H_2O at pH 7 and B) 0.1 M AcOH/Et_3N in 80% (v/v) MeCN in H_2O. Gradient: 0-25% of B in 45 min. Flow rate = 5 ml·min^{-1}. The purified ON was analyzed by RP-HPLC (1260 Infinity II LC System from Agilent equipped with a G7165A detector) using an EC 250/4 Nucleodur 100-3 C18ec from Macherey-Nagel. Gradient: 0-25% or 0-30% of B in 45 min. Flow rate = 1 ml·min^{-1}. Finally, the purified ON was desalted using a C18 RP-cartridge from Waters.

Please cite this article in press as: Bérouti et al., Pseudouridine RNA avoids immune detection through impaired endolysosomal processing and TLR engagement, Cell (2025), https://doi.org/10.1016/j.cell.2025.05.032

The absorbance of the synthesized ON in H_2O solution was measured using an IMPLEN NanoPhotometer® N60/N50 at 260 nm. The extinction coefficient of the single stranded ONs was calculated using the OligoAnalyzer Version 3.0 from Integrated DNA Technologies. For ONs incorporating non-canonical bases, the extinction coefficients were assumed to be identical to those containing only canonical counterparts. The synthesized ON (2-3 μl) was desalted on a 0.025 μm VSWP filter (Millipore), co-crystallized in a 3- hydroxypicolinic acid matrix (HPA, 1 μl) and analyzed by MALDI-TOF mass spectrometry (negative mode).

NMR analysis of ΨΨΨAGC and UUUAGC

Samples of ΨΨΨAGC and UUUAGC were purified by an NaOAc/EtOH precipitation with subsequent desalting by a NAP-5 Sephadex column (Cytiva). Purified oligonucleotides were lyophilized and dissolved in 25 mM sodium phosphate pH 6.4, 25 mM NaCl, 10% D_2O. NMR experiments were recorded on 600 and 1200 MHz Bruker NMR spectrometers equipped with cryogenic probes. 1D ^1H experiments were recorded at 282 K using a WATERGATE flip-back pulse sequence for water suppression. For investigation of non-exchangeable resonances, samples were dissolved in 25 mM sodium phosphate pH 6.4, 25 mM NaCl, 100% D_2O. 1D ^1H experiments were recorded, as well as homonuclear ^1H,^1H-NOESY (mixing time 300 ms) and ^1H,^1H-TOCSY (mixing time 60 ms) experiments. The residual water signal was suppressed using an excitation sculpting sequence. Spectra were processed in TopSpin v.3.5pl7 and analyzed in CCPNMR 2.4.2.

QUANTIFICATION AND STATISTICAL ANALYSIS

Statistical analyses were conducted using Prism 10. The sample sizes (n) and statistical methods, where applicable, are detailed in the respective figure legends.

CellPress
OPEN ACCESS

Supplemental figures

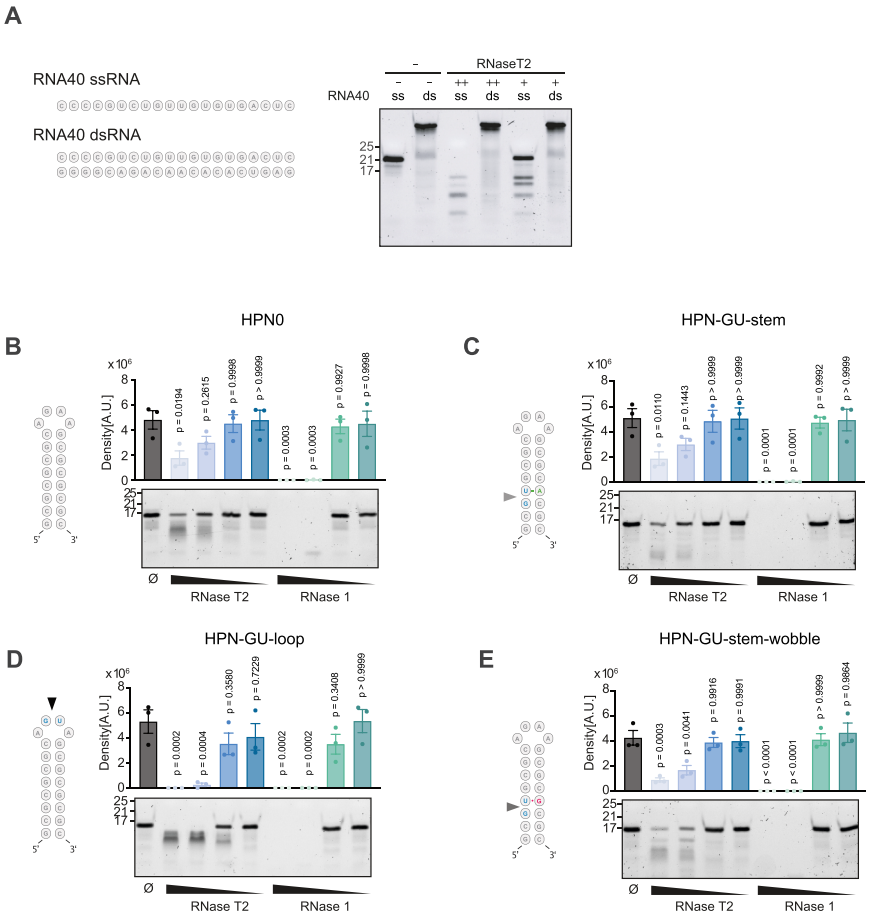

Figure S1. RNase T2 does not cleave dsRNA40, related to Figure 1

(A) Urea gel of ssRNA40 and dsRNA40 digested with RNase T2 (++ = 37 nM, + = 3.7 nM) in IDTE buffer. Data represent two independent experiments.

(B–E) Urea gels of depicted hairpin RNAs digested with RNase T2 (3.7 μM, 0.37 μM, 37 nM, and 0.37 nM) or RNase 1 (0.6 μM, 60 nM, 6 nM, and 0.6 nM) in IDTE buffer. One representative gel of three independent experiments is shown. Top, the quantification of the densitometry analysis of the uncut RNA oligonucleotide for each condition. Data are presented as mean ± SEM from n = 3 independent experiments. Statistical analysis was performed using a one-way ANOVA, comparing the untreated RNA to other conditions with Dunnett's multiple comparisons test.

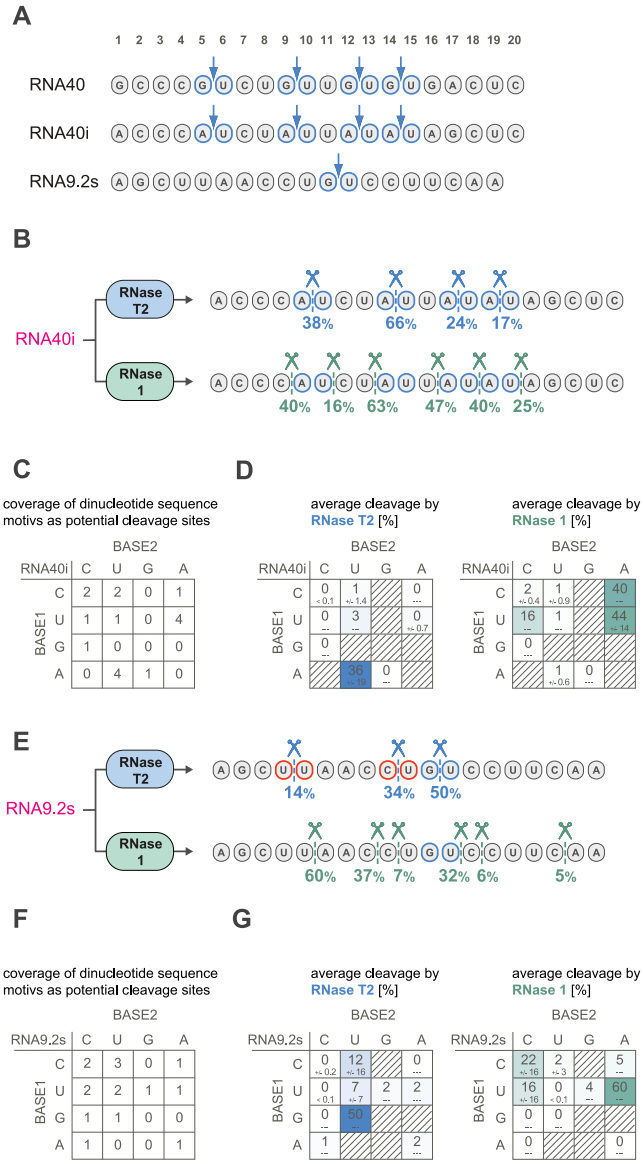

Figure S2. Characterization of RNA40i and RNA9.2s digested with RNase T2 or RNase 1, related to Figure 1

(A) Scheme of RNA40, RNA40i, and RNA9.2s and their major RNase T2 cut sites.

(B) RNA40i (1 µg) was digested with RNase T2 (35 nM) or RNase 1 (3 nM) in IDTE buffer and analyzed by HPLC-HESI-MS. The percentage of cleavage at a given site for RNA40i processed by RNase T2 or RNase 1 is indicated. All sites with >3% cleavage are shown. Data from three independent experiments were summarized.

(C) The coverage of dinucleotide motifs as potential cleavage sites in RNA40i is shown with only internal sites being considered.

(D) Average cleavage percentages for all possible dinucleotide motifs of RNA40i digested with RNase T2 (35 nM) or RNase 1 (3 nM). Data from three independent experiments were summarized and cleavage percentages are depicted as mean values (large letters) + SD (small letters, below).

(E) RNA9.2s (1 µg) was digested with RNase T2 (35 nM) or RNase 1 (3 nM) in IDTE buffer and analyzed by HPLC-HESI-MS. The percentage of cleavage at a given site for RNA9.2s processed by RNase T2 or RNase 1 is indicated. All sites with >4 % cleavage are shown. Data from three independent experiments were summarized.

(F) The coverage of dinucleotide motifs as potential cleavage sites in RNA9.2s is shown with only internal sites being considered.

(G) Average cleavage percentages for all possible dinucleotide motifs of RNA9.2s digested with RNase T2 (35 nM) or RNase 1 (3 nM). Data from three independent experiments were summarized and cleavage percentages are depicted as mean values (large letters) + SD (small letters, below).

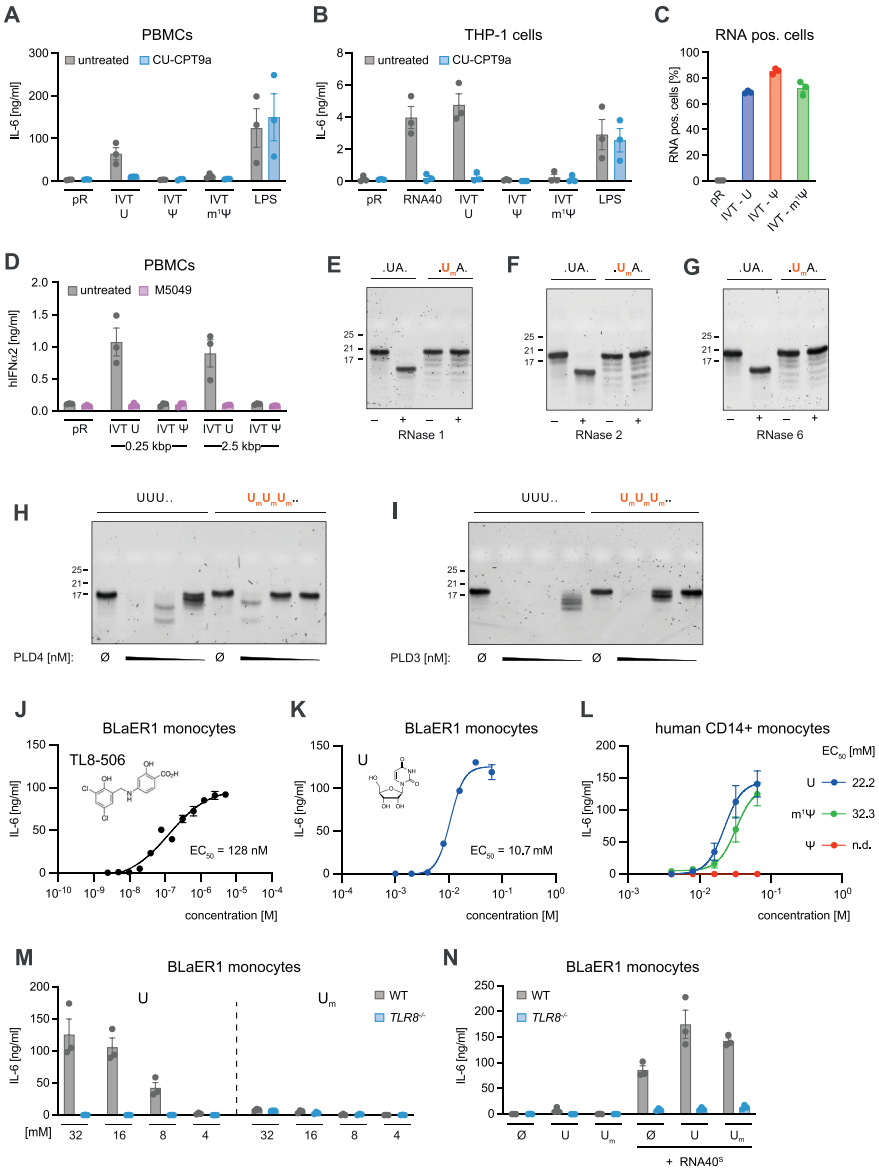

Figure S3. 2′-O-methyluridine is not a substrate for TLR8, related to Figures 4 and 5

(A) PBMCs were stimulated with pR, OVA-U, OVA-Ψ, OVA-m^{1}Ψ, and LPS with or without CU-CPT9a. After 24 h, IL-6 release was measured. Data are depicted as mean ± SEM of *n* = 3 independent donors.

(B) THP-1 cells were stimulated with pR, ssRNA40^S, OVA-U, OVA-Ψ, OVA-m^{1}Ψ, and LPS in the presence or absence of CU-CPT9a. After 14 h, IL-6 release was measured. Data are depicted as mean ± SEM of *n* = 3 independent experiments.

(C) Percentage of AZDye488 percentage-positive BLaER1 monocytes after transfection with pR alone or pR complexed with OVA IVT-U, OVA IVT-Ψ, or OVA IVT-m^{1}Ψ analyzed by FACS. Data are depicted as mean ± SEM of *n* = 3 independent experiments.

(D) PBMCs were stimulated with indicated Cas9 IVT constructs with or without M5049. After 24 h, IFNα2 release was measured. Data are depicted as mean ± SEM of *n* = 3 independent donors.

(E–G) Urea gels of $(dAdC)_7$GAGUAGA and $(dAdC)_7$GAGUmAGA digested with (E) RNase 1 (60 nM), (F) RNase 2 (55 nM), or (G) RNase 6 (60 nM) in assay buffer. One representative blot of two independent experiments is shown.

(H and I) Urea gels of UUUGCUUAACCUGUCCUU and UmUmUmGCUUAACCUGUCCUU digested with (H) PLD4 (250, 25, and 2.5 nM) or (I) PLD3 (25, 2.5, and 0.25 nM) in assay buffer. One out of two independent experiments is shown.

(J and K) BLaER1 monocytes were stimulated with increasing concentrations of (J) TL8-506 or (K) U. After 14 h, IL-6 release was measured. Each replicate of *n* = 3 independent experiments is depicted. A four-parameter dose-response curve was fitted to calculate half-maximal effective concentration (EC_{50}).

(L) CD14$^+$ monocytes were stimulated with increasing concentrations of U, Ψ, or m^{1}Ψ for 24 h. Afterward, IL-6 release was detected. Data are depicted as mean ± SEM of *n* = 3 independent donors. A four-parameter dose-response curve was fitted to calculate half-maximal effective concentration (EC_{50}).

(legend continued on next page)

(M) Wild-type and TLR8$^{-/-}$ BLaER1 monocytes were stimulated with decreasing concentrations of U or 2′-O-methyluridine as indicated. After 14 h, IL-6 release was detected. Data are depicted as mean ± SEM of n = 3 independent experiments.
(N) BLaER1 cells of indicated genotypes were stimulated with U, 2′-O-methyluridine or in combination with ssRNA40^{S} for 14 h. IL-6 release was subsequently analyzed. Data are depicted as mean ± SEM of n = 3 independent experiments.

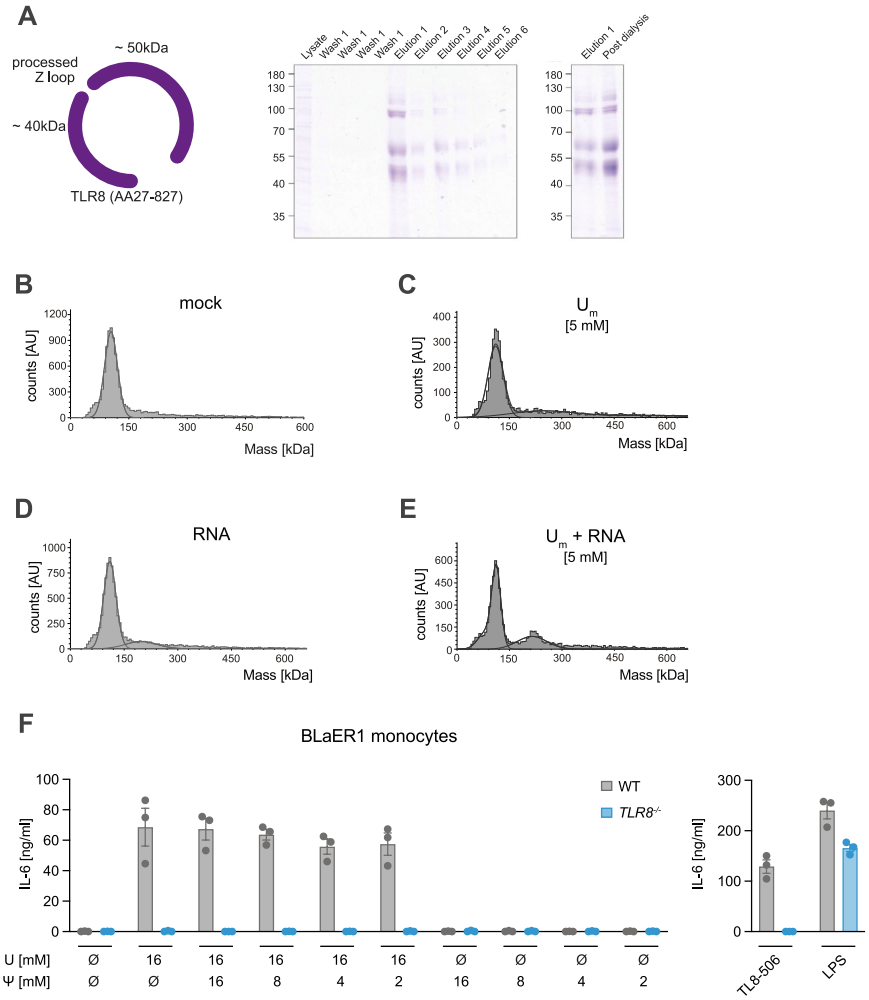

Figure S4. Ψ does not inhibit U binding to TLR8, related to Figure 5

(A) Scheme of hsTLR8 (AA27-827) after cleavage of the Z-loop and Coomassie gels of the EPEA bead purification of hsTLR8 (aa27–827) and of hsTLR8 (aa27–827) after buffer exchange by dialysis.

(B) Mass distribution of hsTLR8 (aa27–827) observed by mass photometry.

(C) Mass photometry analysis of hsTLR8 (aa27–827) incubated with ssRNA40^{O}.

(D) Mass photometry analysis of hsTLR8 (aa27–827) incubated with 5 mM Um.

(E) Mass photometry analysis of hsTLR8 (aa27–827) incubated with 5 mM Um and ssRNA40^{O}.

(F) Wild-type and TLR8$^{-/-}$ BLaER1 monocytes were unstimulated or stimulated with U, a combination of U and Ψ, TL8-506, or LPS. After 14 h, IL-6 release was measured. Data are depicted as mean ± SEM of n = 3 independent experiments.

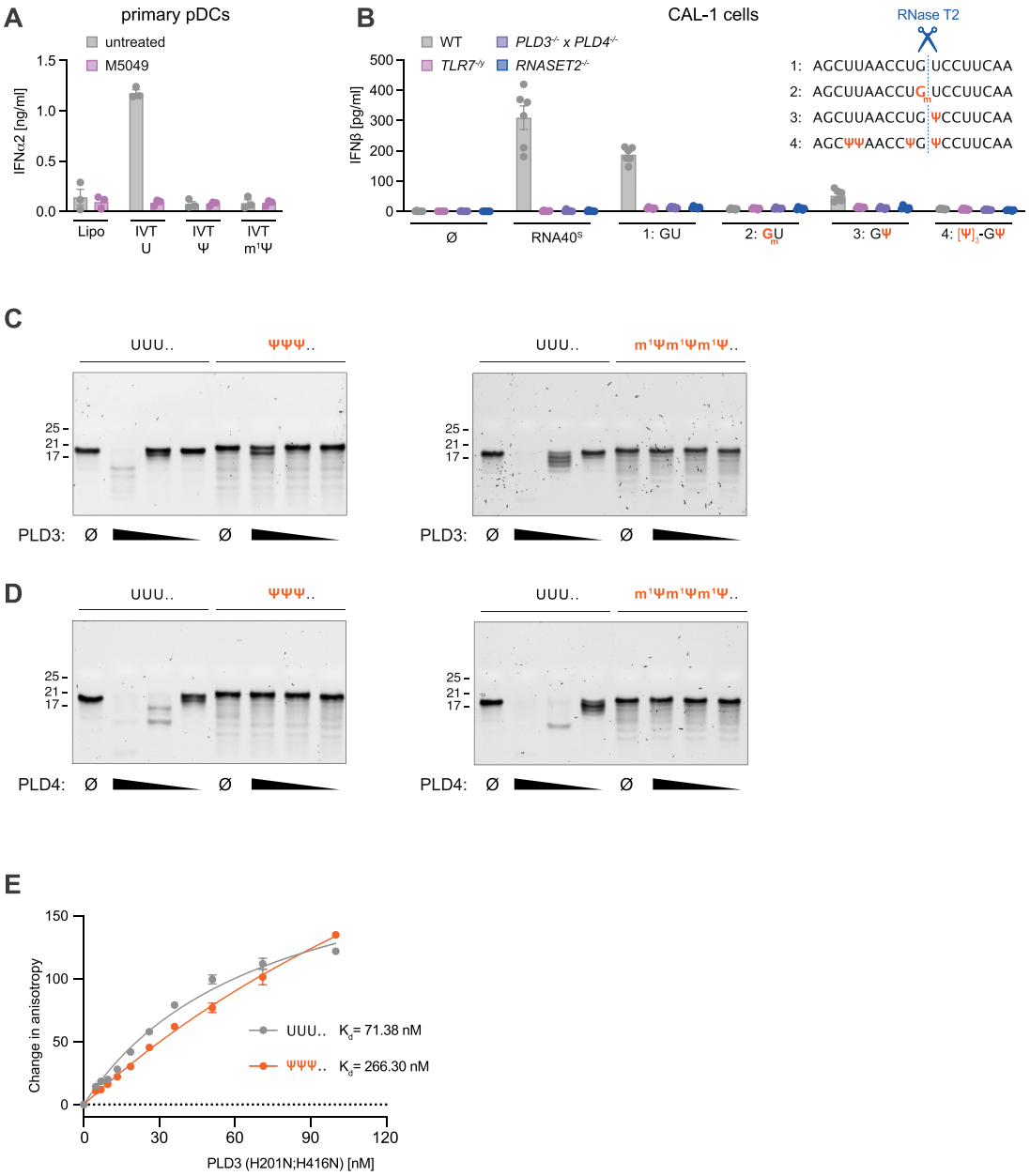

Figure S5. Ψ inhibits cleavage by PLD exonucleases, related to Figure 6

(A) pDCs were stimulated with lipofectamine only or with OVA-U, OVA-Ψ, and OVA-m^{1}Ψ with or without M5049. After 24 h, IFNα2 release was measured. Data are depicted as mean ± SEM of n = 3 independent donors.

(B) CAL-1 cells of indicated genotypes were stimulated as indicated. After 16 h, IFN-β release was determined. Data are depicted as mean ± SEM of n = 6 independent experiments.

(C) Urea gels of UUUGCUUAACCUGUCCUU, ΨΨΨGCUUAACCUGUCCUU, and m^{1}Ψm^{1}Ψm^{1}ΨGCU-UAACCUGUCCUU digested with PLD3 (2.5, 0.25, and 0.025 nM) in assay buffer. One out of two independent experiments is shown.

(D) Urea gels of UUUGCUUAACCUGUCCUU, ΨΨΨGCUUAACCUGUCCUU, and m^{1}Ψm^{1}Ψm^{1}ΨGCU-UAACCUGUCCUU digested with PLD4 (250, 25, and 2.5 nM) in assay buffer. One out of two independent experiments is shown.

(E) Fluorescence anisotropy assay assessing the binding of PLD3$^{H201N,\ H416N}$ at increasing concentrations to UUUGCUUAACCUGUCCUU and ΨΨΨGCUUAACCUGUCCUU. Data are shown as mean ± SEM of n = 3 independent experiments.

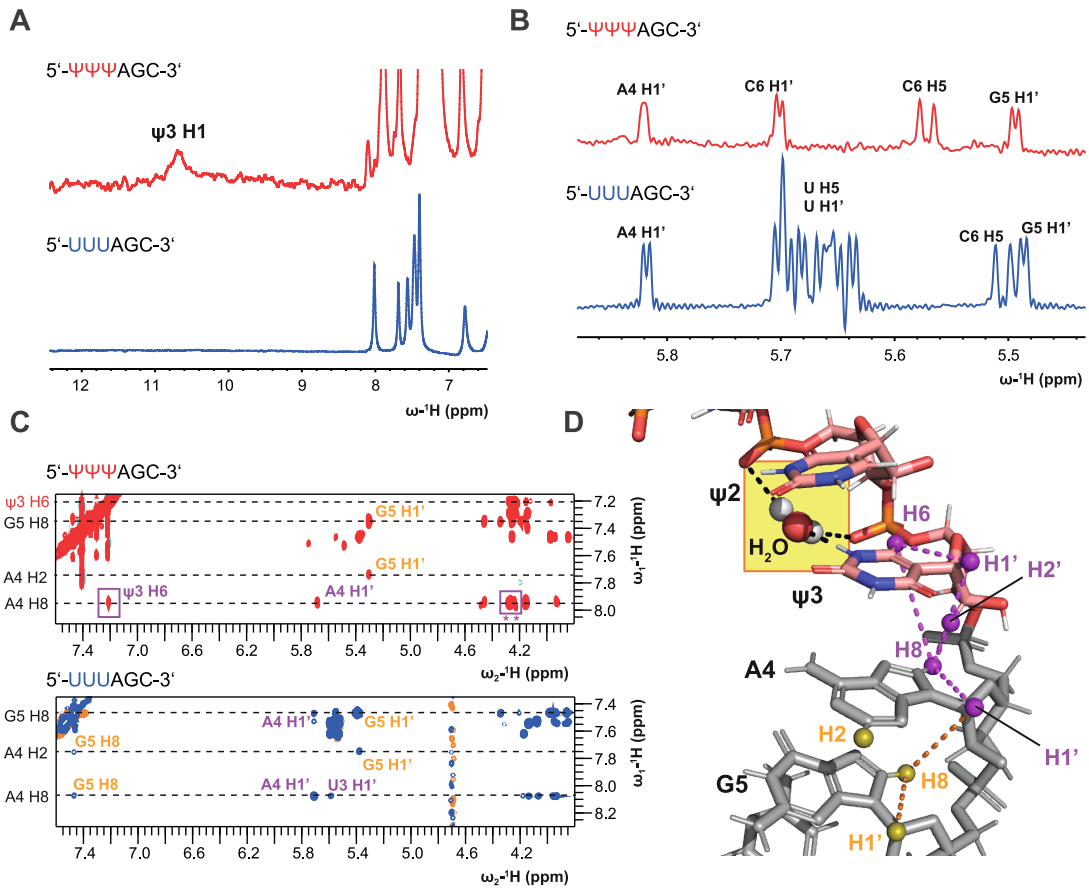

Figure S6. Ψ-RNA adopts an A-form conformation, related to Figure 6

(A) 1D ^{1}H NMR spectra of the imino region of ΨΨΨAGC (highlighted in red) and UUUAGC (highlighted in blue) revealing an additional H1 signal in ΨΨΨAGC most likely corresponding to Ψ3. Spectra were recorded at 600 MHz, 282 K.

(B) 1D ^{1}H NMR spectra of the H1′ region of the ribose's of ΨΨΨAGC and UUUAGC indicating a smaller splitting due to the 3J(H1′, H2′) coupling of the A4 and G5 signals (≈1–2 Hz) compared with the spectrum of the UUU-oligo (≈3 Hz). The smaller coupling in ΨΨΨAGC suggests a higher population of C3′endo conformation for the ribose of A4. Spectra were recorded at 600 MHz, 282 K for UUUAGC and 293 K for ΨΨΨAGC.

(C) Anomeric-aromatic region of ^{1}H,^{1}H NOESY spectra recorded at 600 MHz for UUUAGC and 1,200 MHz for ΨΨΨAGC. Both NMR spectra were recorded at 282 K with a mixing time of 300 ms. NOEs of A4 to U3/Ψ3 are annotated in purple, NOEs to G5 in yellow. An NOE from A4H8 to Ψ3H6 indicates base stacking. A corresponding NOE could not be observed in UUUAGC, suggesting a higher structural stabilization in ΨΨΨAGC. Two NOEs to the Ψ3 ribose were observed (marked by asterisks), which could not be further assigned.

(D) The NOEs are shown in a structural model of ΨΨΨAGC with A-form geometry. The model was generated using RNA composer. The imino H1 proton of Ψ3 is stabilized by a water-mediated H-bond to its own phosphate and the phosphate of the 5′ nucleotide (yellow box).